*Economic Geology*, v. XXX, no. XX, pp. X–X

# Complex Effects of Assimilation on Sulfide Saturation Revealed by Modeling with the Magma Chamber Simulator: A Case Study on the Duluth Complex, Minnesota, USA

Ville J. Virtanen,[1,†] Jussi S. Heinonen,[1] Nicholas D. Barber,[2] and Ferenc Molnár[3,*]

[1]*University of Helsinki, Department of Geosciences and Geography, Helsinki FI-00014, Finland*

[2]*University of Cambridge, Department of Earth Sciences, Cambridge CB2 3EQ, UK*

[3]*Geological Survey of Finland, Espoo 02151, Finland*

## Abstract

Wall-rock assimilation can cause effective sulfide saturation in magmas and lead to the formation of base and precious metal sulfide deposits. Detailed assessments of how assimilation affects the sulfur content at sulfide saturation (SCSS) in magmas have been scarce because of the lack of suitable thermodynamic modeling tools. The Magma Chamber Simulator (MCS) is the first geochemical modeling software that accounts for thermodynamic wall-rock phase equilibrium in open magmatic systems experiencing recharge-assimilation-fractional crystallization. We used the MCS to model SCSS in a magmatic system corresponding to the parental melt of the Partridge River intrusion of the Duluth Complex, Minnesota. This intrusion hosts several Cu-Ni deposits in troctolitic and noritic rocks, which both show evidence of assimilation of the adjacent Virginia Formation black shale. Our simulations show that the dominantly troctolitic rocks can form via fractional crystallization if the parental melt is hydrous (≥1 wt % $H_2O$), while gabbroic rocks dominate when the parental melt is $H_2O$ poor (≤0.14 wt % $H_2O$). Formation of norite from the hydrous parental melt requires ~20–30% of selective assimilation of black shale partial melts or bulk assimilation of stoped blocks. In the fractional crystallization simulations, increasing the $H_2O$ content of the parental melt lowers SCSS. In the hydrous fractional crystallization scenarios, SCSS is lowered further by the depletion of FeO from the residual melt, owing to enhanced olivine stability. In the assimilation simulations, the residual melt in the magma subsystem becomes enriched in $SiO_2$, $Al_2O_3$, $K_2O$, and $H_2O$ with simultaneous depletion in FeO, MgO, CaO, and $Na_2O$. These compositional changes promote sulfide saturation—an effect that is more pronounced in selective rather than in bulk assimilation scenarios.

Trace element models, used as a proxy for the efficiency of sulfur assimilation, show that sulfur should behave as an incompatible element ($D^{WR}$ (S) ≤ 1) to wall rock in the selective assimilation simulations, i.e., enriched in early-assimilated wall-rock fluids and/or partial melts, in order to fulfill the natural sulfur isotope criteria of the Duluth Complex. Bulk assimilation may also be efficient enough to modify the sulfur isotope composition, but it requires a large amount of crystallization in the magma and is, hence, considered less likely to be the main process for sulfur assimilation. If wall-rock sulfur is effectively transported to the magma, in situ precipitation of sulfides without notable subsequent upgrading by dynamic processes could produce the sulfide grade of an average Cu-Ni deposit in the Partridge River intrusion.

## Introduction

Timing and degree of sulfide saturation are parameters that largely control the economic potential of magmatic systems. The maximum amount of sulfur that a silicate melt can dissolve before it becomes saturated in an immiscible sulfide phase is defined as sulfur content at sulfide saturation (SCSS; Shima and Naldrett, 1975; for a comprehensive review see O'Neill, 2021). The SCSS is defined by experimentally calibrated equations, in which the common variables are temperature, pressure, oxygen fugacity, and a set of major element oxides (including $H_2O$) in the host silicate melt (e.g., Liu et al., 2007; Li and Ripley, 2009; Jugo et al., 2010; Fortin et al., 2015). In addition, the composition of the sulfide phase (Fe, Cu, Ni, and S) has been shown to affect the SCSS (Smythe et al., 2017). At crustal levels, closed magmatic systems reach sulfide saturation via cooling and crystallization. Sulfides form in cotectic proportions, but the concentrations are rarely sufficient for economical exploitation (e.g., Ripley and Li, 2013).

Wall-rock assimilation has been identified as the decisive process leading to efficient sulfide saturation and formation of many magmatic Ni-Cu-platinum group element (PGE) sulfide deposits hosted by layered intrusions and komatiitic lavas (Ripley and Li, 2003, 2013; Naldrett, 2010; Barnes et al., 2016; Lesher, 2019). Some of the most notable examples include world-class Ni-Cu(-PGE) deposits such as Norilsk in Russia, Voisey's Bay in Canada, Kambalda in Australia, and Duluth Complex in the United States (Mainwaring and Naldrett, 1977; Naldrett, 1999, 2010; Ripley et al., 1999a; Ripley and Li, 2013; Lesher, 2019). Assimilation can promote the formation of an immiscible sulfide phase from the magma in multiple ways: (1) increasing the total sulfur content of the magma, (2) lowering the SCSS as the major element composition of the silicate melt changes, (3) changing sulfide composition, and (4) reducing dissolved sulfate to sulfide (Ripley and Li, 2013; Iacono-Marziano et al., 2017).

Traditionally, in simulations of assimilation-induced effects on SCSS in Ni-Cu(-PGE) systems, components like wall rock,

†Corresponding author: e-mail, ville.z.virtanen@helsinki.fi

*Current address: Eötvös Loránd University, Department of Mineralogy, Institute of Geography and Earth Sciences, 1117 Budapest, Pázmány Péter s. 1/C, Hungary.

ISSN 0361-0128; doi:10.5382/econgeo.4917; 19 p.
Digital appendices are available in the online Supplements section.

hypothetical partial melt, and/or fluid are added to the magma as a bulk component in a single chemical mixing event, often without considerations of wholesale mass balance (see e.g., Ripley and Li, 2013). More often, the effects of assimilation on SCSS are considered only qualitatively by speculating how the addition of specific oxide components (e.g., $SiO_2$, $K_2O$, or $H_2O$) would affect the SCSS (Irvine, 1975; Li and Naldrett, 2000; Liu, Y., et al., 2017). While these considerations serve as a qualitative first-order approximation of how assimilation affects SCSS in magma, they neglect the heat and mass balance, thermodynamic phase equilibria, and progressive nature of the assimilation process. In nature, assimilation is inherently coupled with crystallization, which causes continuous and often nonlinear solid-melt mass fluxes in the magma (e.g., Bohrson et al., 2014; Heinonen et al., 2021). Simultaneously, phase equilibrium in the progressively heated wall rock dictates the composition of the assimilated material (e.g., Bohrson et al., 2014; Heinonen et al., 2021). Recent developments in thermodynamically constrained modeling tools for open magmatic systems (for a review, see Heinonen et al., 2021) has enabled elaborate assimilation simulations. Only recently, have these tools been applied to study sulfide saturation in Ni-Cu(-PGE) crystallizing systems (e.g., Yao and Mungall, 2021).

In this contribution, we use the Magma Chamber Simulator (MCS; Bohrson et al., 2014; 2020) software to simulate fractional crystallization (FC), assimilation-fractional crystallization (AFC), and stoping-fractional crystallization (SFC) in a magmatic system that corresponds to the well-studied Cu-Ni–mineralized Partridge River intrusion of the Duluth Complex, Minnesota. We combine the outcomes of the MCS simulations with the SCSS model of Smythe et al. (2017) to show how the SCSS of the magmas going through FC, AFC, and SFC processes differ from each other. Although we use Partridge River intrusion as our case study, our purpose is not to create a comprehensive model for its specific magmatic evolution or mineralization. Rather, we aim to demonstrate the power and utility of thermodynamically constrained open-system magmatic modeling as applied to Ni-Cu–critical magmatic systems, in the hope that a similar approach can be adopted more widely in the research related to these systems.

## Geologic Setting of the Duluth Complex

### *Igneous rocks and sulfide deposits*

The Duluth Complex, Minnesota (Fig. 1), is a large (>5,500 km$^2$) assemblage of dominantly mafic intrusions that were emplaced underneath the cogenetic continental flood basalts of the North Shore Volcanic Group (Miller et al., 2002). Overall, the magmatic event extended from 1109 to 1084 Ma, but the bulk of the Duluth Complex formed in less than a million years at ~1096 Ma (Swanson-Hysell et al., 2021). This main stage of magmatism is manifested by the Anorthositic and Troctolitic Series layered intrusions (Fig. 1), named after their characteristic rock types (e.g., Miller et al., 2002). A variety of ultramafic, gabbroic, and noritic rocks are also present, and locally dominant, in both the Anorthositic and Troctolitic Series intrusions (e.g., Rao and Ripley, 1983; Miller and Ripley, 1996; Miller et al., 2002; Ripley et al., 2007; Queffurus and Barnes, 2014). Pegmatitic troctolites are also present locally (Severson and Barnes, 1991; Ripley et al., 1993; Severson et al., 1996).

The rock names used henceforward comply with the terminology of Phinney (1972), which has been historically widely applied to the Duluth Complex (e.g., Miller and Weiblen, 1990; Severson et al., 1996; Miller et al., 2002). The Troctolitic Series intrusions formed by emplacement of multiple consecutive sheets of olivine ± plagioclase-bearing magmas (Miller and Ripley, 1996; Ripley et al., 2007). The generation of the associated rock types, from peridotites to various troctolitic and gabbroic rocks, has been attributed to the varying dominance of fractional crystallization, crystal accumulation, and equilibrium crystallization (Chalokwu et al., 1993; Miller and Ripley, 1996; Ripley et al., 2007). The peridotites and troctolites are meso- and orthocumulates and formed by the compaction of the olivine ± plagioclase phenocrysts, whereas the gabbroic rocks formed via equilibrium crystallization from the expulsed residual melt (Chalokwu et al., 1993; Ripley et al., 2007). The typical crystallization sequence is olivine → plagioclase + olivine → plagioclase + olivine + clinopyroxene ± orthopyroxene (Miller and Ripley, 1996; Miller et al., 2002). Plagioclase with anorthite (An) content between $An_{85}$ and $An_{35}$ typically constitutes 50–80 vol % of the troctolites and gabbros (Mainwaring and Naldrett, 1977; Rao and Ripley, 1983; Chalokwu et al., 1993; Lee and Ripley, 1996; Miller et al., 2002; Ripley et al., 2007). Olivine composes 10–30 vol % of the troctolites and gabbros and reaches 70 vol % in the peridotitic rocks. Olivine composition ranges from forsterite (Fo) content $Fo_{71}$ to $Fo_{29}$ (Rao and Ripley, 1983; Lee and Ripley, 1996; Miller and Ripley, 1996; Miller et al., 2002; Ripley et al., 2007), but the primary forsterite contents were approximately $Fo_{56–79}$ before equilibration with the trapped liquid (Chalokwu et al., 1993). The clinopyroxene, with Mg# generally between 40 and 80, is mostly interstitial, and its modal proportion is typically 0–20 vol %, but in a few meter-scale layers clinopyroxene is oikocrystic and reaches modal proportions up to 90 vol % (Rao and Ripley, 1983; Miller et al., 2002; Ripley et al., 2007). Magmatic biotite (up to 8 vol %) is a common interstitial phase in the intrusions, indicating that the magmas were hydrous (Weiblen and Morey, 1980; Saini-Eidukat et al., 1990; Ripley et al., 1993, 2007).

Norites are volumetrically minor, and they are mainly present along the contacts to the Virginia Formation black shale footwall and xenoliths (Rao and Ripley, 1983; Thériault and Barnes, 1998; Ripley et al., 2007; Queffurus and Barnes, 2014; Samalens et al., 2017). The presence of black shale footwall and xenoliths with restitic minerals and recrystallized partial melt has been taken as evidence that the norites formed when the Duluth Complex parental melt assimilated black shale partial melts (Ripley and Alawi, 1986; Thériault and Barnes, 1998; Queffurus and Barnes, 2014; Samalens et al., 2017). The absence of sharp compositional gradients around the restitic xenoliths implies that the partial melt assimilation occurred when the magma was mostly molten and widespread chemical mixing was possible (Ripley and Alawi, 1986).

Sulfides are common minor constituents of most of the rock types in the Duluth Complex. The basal Troctolitic Series intrusions of the Duluth Complex host ~10 known magmatic Cu-Ni(-PGE) sulfide deposits (Fig. 1) with a combined tonnage of 4.4 billion tons (Gt) at 0.66 wt % Cu and 0.2 wt % Ni

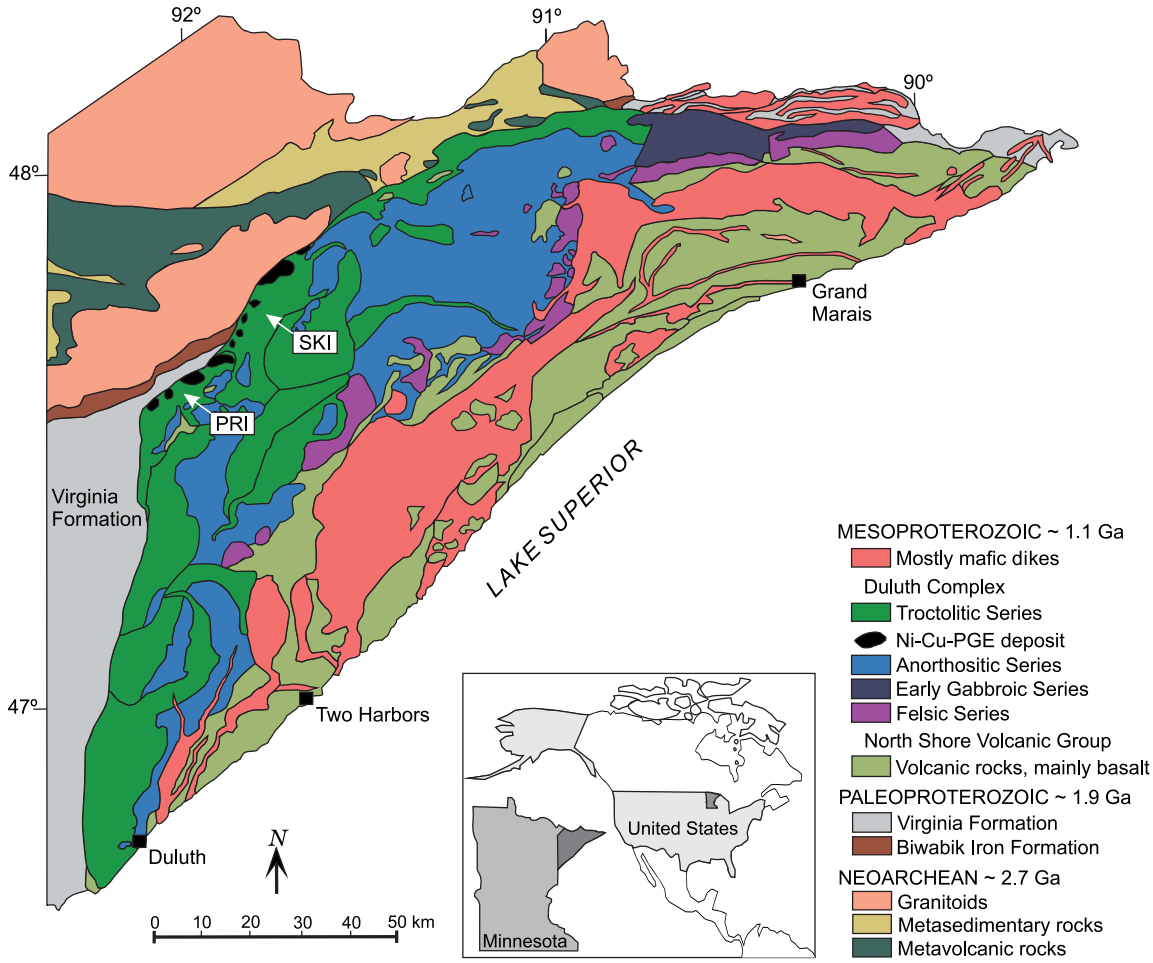


Fig. 1. A geologic map of the Duluth Complex, Minnesota, and the adjacent bedrock. PGE = platinum group element, PRI = Partridge River intrusion, SKI = South Kawishiwi intrusion. Modified after Benkó et al. (2018).

(Listerud and Meineke, 1977; Miller et al., 2002). Troctolites host ~70% of the deposits, while the rest are present within norites and the black shale footwall and xenoliths (Severson and Barnes, 1991; Miller et al., 2002). Sulfur isotope data suggest that the Virginia Formation black shale acted as a main source of sulfur for many of the sulfide deposits (Mainwaring and Naldrett, 1977; Ripley, 1981; Andrews and Ripley, 1989). The troctolite-hosted disseminated Cu-Ni sulfide deposits in the Partridge River intrusion have likely formed by selective assimilation of sulfur-rich fluids and/or melts from the Virginia Formation black shale (Ripley, 1981; Rao and Ripley, 1983; Tyson and Chang, 1984; Thériault and Barnes, 1998; Ripley et al., 2007). The selective nature of sulfur assimilation is evident as Sr, Pb, and Nd isotope composition of the troctolites constrains bulk assimilation to ≤5 wt %, which cannot explain the sulfur mass balance (Grant and Molling, 1981; Ripley et al., 1999b). The norite-hosted deposits with disseminated and massive sulfides show evidence of more extensive assimilation, and they likely formed by the introduction of sulfides via silicate partial melts from Virginia Formation xenoliths (Thériault and Barnes, 1998; Queffurus and Barnes, 2014; Samalens et al., 2017). Radiogenic isotopic data of the norites is scarce compared to the troctolites, but oxygen isotopes indicate that black shale assimilation is generally more than 20 wt % (Ripley et al., 2007).

### *Virginia Formation black shale wall rock*

The Virginia Formation black shale (Fig. 1) is mostly composed of kerogen- and sulfide-bearing argillites with quartz, muscovite, chlorite, and albitic plagioclase as the main minerals (Bonnichsen, 1975; Ripley et al., 2001). The Virginia Formation has been contact metamorphosed by the Duluth Complex magmas (Bonnichsen, 1975; Severson et al., 1996; Sawyer, 2014). In the distal part of the contact aureole, biotite and cordierite partially replace muscovite and chlorite due to subsolidus devolatilization reactions (Sawyer, 2014). A metatexitic migmatite zone marks the onset of partial melting of biotite, feldspar, and quartz (Sawyer, 2014). The primary bedding is mainly preserved in this zone, indicating that the degree of partial melting was too low for significant melt percolation (Sawyer, 2014). The degree of partial melting increases toward the contact in the diatexite migmatite zone and in the xenoliths, where continuous melt networks were present (Sawyer, 2014) and partial melt expulsion was possible. This zone records gradational phase changes, including formation of orthopyroxene, complete melting of biotite,

K-feldspar, and quartz, and finally orthopyroxene (Bonnichsen, 1975; Sawyer, 2014). Estimates of the maximum temperature of metamorphism range from ~870 to ~920°C (Holness and Sawyer, 2008; Sawyer, 2014; Benkó et al., 2015) and pressure from 150 to 300 MPa (Bonnichsen, 1975; Frost et al., 2007; Sawyer, 2014).

## Thermodynamic Modeling

Brief descriptions of the thermodynamic and SCSS modeling performed in this work are given here and summarized in Figure 2. A comprehensive description of the modeling software, reasoning behind each input parameter, and the input and output files for each simulation are included in Appendices 1 and 2. To simulate the phase equilibria and major element compositions, we used the MCS (Bohrson et al., 2014, 2020; Heinonen et al., 2020), which is coupled with the thermodynamic engine of the rhyolite-MELTS software (Ghiorso and Sack, 1995; Gualda et al., 2012; Ghiorso and Gualda, 2015; for a detailed description, see App. 1). All the simulations were conducted at 200 MPa pressure, which is in the range of estimated emplacement pressures of the stratigraphically lowest Duluth Complex intrusions (Bonnichsen, 1975; Frost et al., 2007; Sawyer, 2014). We selected a parental melt composition KEW-6 (Basaltic Volcanism Study Project, 1981) from the cogenetic North Short Volcanic Group volcanic rocks for the troctolite-dominated intrusions of the Duluth Complex (Table 1). We conducted 12 closed-system FC simulations with various initial $H_2O$ contents (dry, 0.14, 1, and 2.25 wt %) and oxygen fugacity ($f_{O_2}$) conditions (Fig. 2). The initial $f_{O_2}$ buffers, and hence the $FeO/Fe_2O_3$ of the parental melt (App. 1, Table A1), were determined to be at the fayalite-magnetite-quartz buffer ($\Delta FMQ_i$ 0; the lowercase i denotes initial) as well as at one ($\Delta FMQ_i$ –1) and two ($\Delta FMQ_i$ –2) log units lower than the FMQ buffer. The rock types, formed via perfect crystal accumulation during 80 mass units (m.u.) of crystallization (total system mass 100 m.u.) in the simulations, are compared with a stratigraphical column (Fig. 3) from the unit IV of the Partridge River intrusion representing uncontaminated troctolites (Severson et al., 1996). The chemistry of the solids and melt in the simulation that we considered the most plausible for the unit IV of the Partridge River intrusion are compared with natural cumulate compositions (see below). Similar comparisons are provided for three other Duluth Complex parental melt compositions (Miller and Weiblen, 1990; Chalokwu et al., 1996; Lee and Ripley, 1996) in Appendix 1.

We used the model of Smythe et al. (2017) to determine the SCSS in the FC simulations defined in Figure 2. Ripley and Li (2013) used an S content of 800 ppm for the Duluth Complex parental melt and considered S as a completely incompatible element with respect to the crystallizing silicates and oxides in the magma. Accordingly, we adopted a parental melt S content of 800 ppm for our simulations and used a bulk partition coefficient of 0.001 between the crystallizing solids and the residual melt. A static bulk sulfide composition for the simulations (38.2% Fe, 8.6% Cu, 2.9% Ni, and 50.3% S) was tentatively estimated using the average composition of the Duluth Complex Cu-Ni deposits (Listerud and Meineke, 1977). Modeling a dynamic sulfide composition would require knowledge of Cu and Ni contents and partition coefficients for the phases present in the parental melt and wall rock as well as incorporation of a thermodynamic model for sulfides, which is out of the scope of this study.

The parental melt which by visual estimation produced the best fit with the natural data in the FC simulations (i.e., $H_2O$ = 1 wt %, $f_{O_2}$ = $\Delta FMQ_i$ –2), was selected as the starting composition for both the AFC and SFC simulations (Fig. 2). A representative black shale composition from the Virginia Formation outside the contact aureole (VF-BS1; Table 1) was chosen for the wall rock. For the AFC simulations, we tested wall-rock masses of 50 and 100 m.u. as well as initial wall-rock

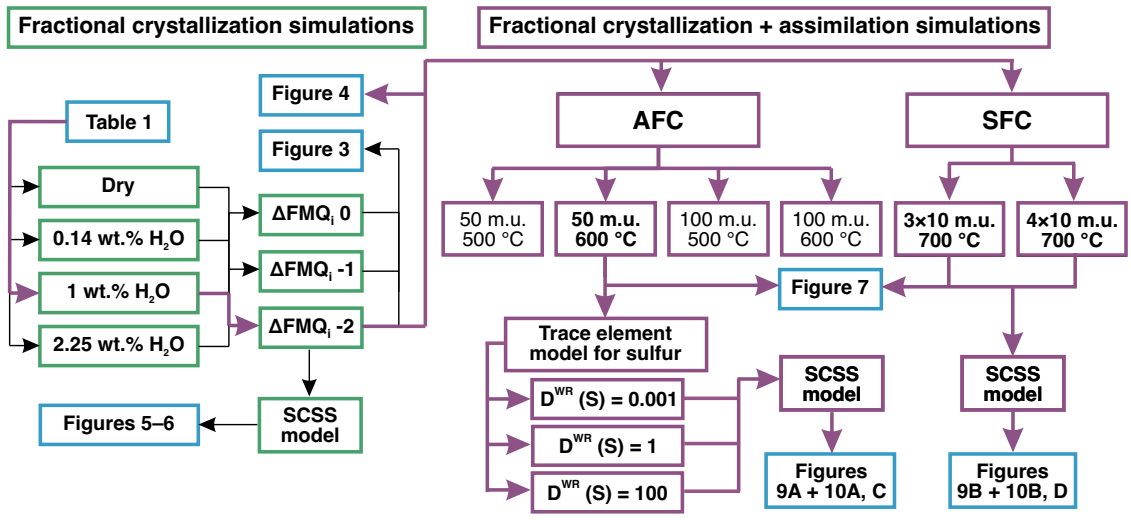


Fig. 2. A flow chart summarizing the conducted Magma Chamber Simulator and sulfur content at sulfide saturation (SCSS) simulations and illustrations (blue boxes) related to each simulation. Twelve fractional crystallization simulations (green boxes) were conducted with different $H_2O$ contents and initial $f_{O_2}$ conditions. The purple arrows track the parental melt used in the assimilation-fractional crystallization (AFC) and stoped block bulk assimilation-fractional crystallization (SFC) simulations. The $D^{WR}$ (S) stands for the sulfur bulk partition coefficient between the wall-rock residual and partial melt. FMQ = fayalite-magnetite-quartz buffer, m.u. = mass unit.

Table 1. Natural Compositions Used to Determine the Parental Melt and Wall-Rock Compositions for the Magma Chamber Simulator Simulations

| | KEW-6[1] | VF-BS1[2] | Black shale (avg)[3] |
|---|---|---|---|
| $SiO_2$ (wt %) | 48.52 | 62.31 | 60.39 |
| $TiO_2$ | 0.72 | 0.70 | 1.00 |
| $Al_2O_3$ | 17.57 | 15.02 | 16.76 |
| $Cr_2O_3$ | 0.05 | n.d. | n.d. |
| $Fe_2O_3$ | 2.18 | 1.60 | n.d. |
| FeO | 6.1 | 4.77 | 7.90 |
| MnO | 0.13 | 0.0580 | n.d. |
| MgO | 8.65 | 3.05 | 3.41 |
| CaO | 9.44 | 0.63 | 0.63 |
| $Na_2O$ | 2.57 | 2.05 | 2.05 |
| $K_2O$ | 0.17 | 3.09 | 3.34 |
| $P_2O_5$ | 0.03 | 0.132 | n.a. |
| $H_2O$ | 2.25 | 3.66 | 3.92 |
| $C_{organic}$ | n.d.[4] | 1.08 | n.d. |
| $C_{inorganic}$ | n.d. | 0.13 | n.d. |
| $CO_2$ | 0.00 | n.d. | n.d. |
| Total | 98.38 | 98.28 | 99.40 |
| S (ppm) | 100 | 3,690 | 6,000 |
| Ce | 6.8 | 65.2 | |

n.d. = no data available

[1]Olivine tholeiite from the North Shore Volcanic Group (Basaltic Volcanism Study Project, 1981)

[2]Virginia Formation black shale sample VF-BS1 from drill core MDDP2 (Virtanen et al., 2021)

[3]Average composition of eight samples from drill core MDDP2 (Rao and Ripley, 1983)

temperatures of 500° and 600°C (Fig. 2). In these simulations, the degree of wall-rock partial melting is constrained by the cooling and crystallizing host magma. The proportion of the wall-rock partial melt that surpasses the percolation threshold of 10 wt % is introduced to the magma. Only the best fit simulation is described in detail (Fig. 2), but all the input and output files from the AFC simulations are available in Appendix 2. In the SFC simulations, the wall-rock material was preheated to 700°C and bulk assimilated to the magma in three ($S_3$FC) or four ($S_4$FC) stoping events (Fig. 2). Each stoping event introduced 10 m.u. of wall-rock material to the magma. The rock sequences formed in the assimilation simulations are compared with a stratigraphical column from unit I of the Partridge River intrusion, which shows signs of assimilation.

For the SCSS models of the AFC and SFC simulations, we used the same parental melt parameters as for the FC simulation. An estimated average S content of the Virginia Formation black shale, 6,000 ppm (Rao and Ripley, 1983; Table 1), was adopted for the wall-rock material. With the current lack of comprehensive thermodynamic models for sulfides, we used the trace element protocol of the MCS (Heinonen et al., 2020) as a tentative proxy for sulfur mobilization and transportation in the AFC simulations. We selected suitable bulk partition coefficients between the wall-rock residual (minerals + fluid) and partial melt, $D^{WR}$ (S), of 0.001, 1, and 100 (Fig. 2). These bulk partition coefficients combine partition coefficients of all phases and are explained in Appendix 1.

## Results of the Thermodynamic Modeling

### *Fractional crystallization simulations*

The rock types formed in the FC simulations are described following the rock classification of Phinney (1972). With dry parental melt and $f_{O_2}$ at $\Delta FMQ_i$ 0, a small mass of anorthosite forms first, which is followed by anorthositic troctolite (± orthopyroxene), and gabbro (Fig. 3). More reducing conditions at $\Delta FMQ_i$ –1 and –2 promote olivine crystallization, which results in a smaller mass of early anorthosite, followed by either anorthositic troctolite or troctolite (Fig. 3). The amount of the dominant gabbro is nearly constant regardless of the initial $f_{O_2}$ conditions (Fig. 3).

The addition of 0.14 wt % $H_2O$ to the parental melt increases the stability of olivine compared to the dry melt with the same initial $f_{O_2}$. The simulation with $f_{O_2}$ at $\Delta FMQ_i$ 0 produces a small mass of anorthosite, which is followed by anorthositic troctolite, troctolite, and norite before the formation of a large mass of gabbro (Fig. 3). With $\Delta FMQ_i$ –1, olivine joins plagioclase as the first crystallizing phase, and consequently the early anorthosite is followed by anorthositic troctolite (Fig. 3). Subsequently, troctolite forms and grades into gabbro (Fig. 3). When the $f_{O_2}$ is set to $\Delta FMQ_i$ –2, the rock sequence consists of troctolite and gabbro (Fig. 3).

The rock sequence produced with the parental melt with intermediate $H_2O$ content of 1 wt % starts with a small mass of dunite (Fig. 3). The dunite is followed by troctolite and then when clinopyroxene stability gradually increases, first by olivine gabbro and then by gabbro (Fig. 3). Finally, gabbro is followed by second troctolite, as olivine becomes stable (Fig. 3). The FC simulation with $f_{O_2}$ at $\Delta FMQ_i$ –1 produces similar stratigraphy but with a higher amount of olivine-bearing rock types (Fig. 3). Because olivine stability further increases with $\Delta FMQ_i$ –2, augite troctolite disappears from the rock sequence (Fig. 3).

All the parental melts with $H_2O$ content of 2.25 wt % produce a rock sequence starting with dunite, which is followed by troctolite, olivine gabbro, and augite troctolite (Fig. 3). The amount of dunite, troctolite, and anorthositic troctolite increases with increasingly reducing initial $f_{O_2}$ (Fig. 3). With the $f_{O_2}$ at $\Delta FMQ_i$ 0 and –1, intermittent norite forms within the augite troctolite (Fig. 3). In the most reduced simulation, norite is absent, although minor orthopyroxene appears briefly in the rock assemblage within the augite troctolite (Fig. 3).

To summarize the results of the rock types formed in the FC simulations: the parental melt compositions with 1 and 2.25 wt % of $H_2O$ and $f_{O_2}$ at $\Delta FMQ_i$ –2 produce the most olivine-rich rocks and hence are the best fits to the natural lithostratigraphy of the Partridge River intrusion (Fig. 3). The minerals produced in the FC simulation with parental melt containing 1 wt % $H_2O$ and $f_{O_2}$ at $\Delta FMQ_i$ –2 are described in more detail here. The presented modal proportions are rounded to the nearest 5 wt % for simplicity, and minor spinel is excluded from the mode. Olivine with $Fo_{84–85}$ is the only silicate present in the dunite. The first troctolite contains 70 wt % of plagioclase with anorthite content ranging from $An_{75}$ to $An_{85}$ and 30 wt % olivine with forsterite content from $Fo_{80}$ to $Fo_{84}$. The amount of plagioclase in the olivine gabbro is 50 wt %, and its anorthite content progressively decreases during the simulation from $An_{74}$ to $An_{69}$. Augite, with Mg# ranging from 75 to 82, composes 40 wt % of the olivine gabbro, while 10 wt % is olivine with composition evolving from $Fo_{68}$ to $Fo_{79}$. The gabbro consists of 45–55 wt % plagioclase with a compositional range from $An_{69}$ to $An_{74}$ and 45–55 wt % of augite and pigeonite with Mg# from 69 to 75 and 57

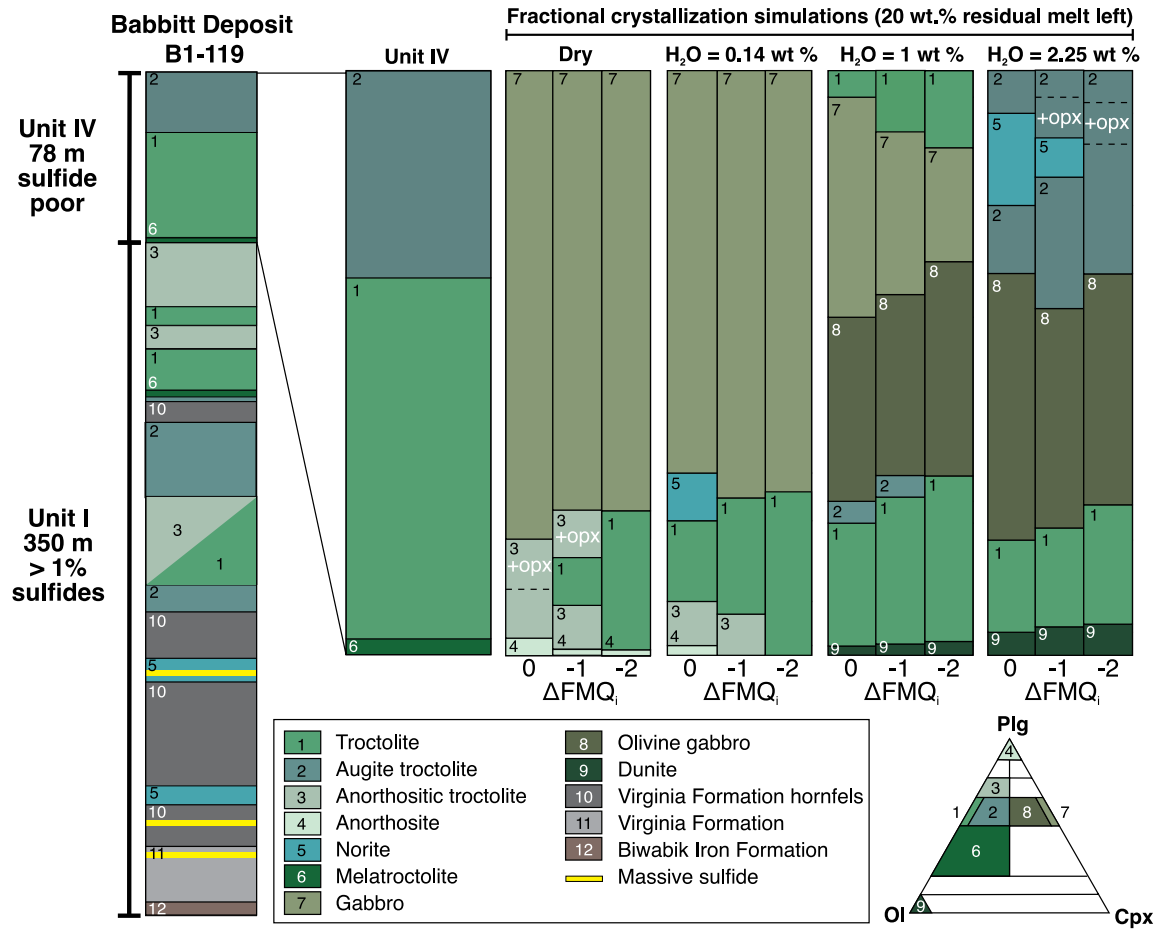


Fig. 3. A natural cumulate sequence of unit IV of the Partridge River intrusion at the Babbitt deposit drill core B1-119 (Severson et al., 1996) and the rock sequences produced with the fractional crystallization simulations (Bohrson et al., 2020) at 20 wt % residual melt left. The unit I was affected by the assimilation of the Virginia Formation black shale. The parental melt compositions were varied in terms of initial $f_{O_2}$ and $H_2O$. Simulated rock sequences were constructed with the help of the Magma Chamber Simulator Visualizer tool (Bohrson et al., 2020). The simulation results illustrate relative masses for different rock types, whereas the drill core illustrates relative volumes—this difference in units has little effect when comparing such mafic compositions. The rock classification diagram with plagioclase (plg), olivine (ol), and clinopyroxene (cpx) is from Phinney (1972). FMQ = fayalite-magnetite-quartz buffer, opx = orthopyroxene.

to 68, respectively. Finally, the late troctolitic rocks are composed of 20–25 wt % of olivine, 60–70 wt % of plagioclase, and 5–10 wt % of clinopyroxene. The troctolite olivine compositions range from $Fo_8$ to $Fo_{52}$, plagioclase composition from $An_{33}$ to $An_{68}$, and clinopyroxene Mg# from 23 to 66. The bulk and incremental solid as well as melt compositions from this FC simulation are shown in Harker diagrams with $Al_2O_3$, $Fe_2O_3^{total}$, MgO, and CaO (Fig. 4), i.e., the dominant major element oxides controlled by olivine, plagioclase, and clinopyroxene. The incremental solid compositions show the composition of solids formed in each simulated 5°C fractionation step, and the bulk composition is a summation of the incremental solids formed.

### *Sulfide saturation in the fractional crystallization simulations*

In the dry magma, sulfide saturation occurs at 37 m.u. crystallization and at the temperature of 1,215°C (Figs. 5, 6). The addition of 0.14 wt % $H_2O$ to the parental melt shifts the sulfide saturation to 29 m.u., and the corresponding temperature is 1,205°C (Figs. 5, 6). The parental melt with 1 wt % of $H_2O$ reaches sulfide saturation at 13 m.u. crystallization and at the temperature of 1,170°C (Figs. 5, 6). In the most hydrous parental melt with 2.25 wt % $H_2O$, sulfide saturation takes place at 3 m.u. crystallization, while the temperature is 1,145°C (Figs. 5, 6). In summary, with increasing initial $H_2O$ both the temperature at sulfide saturation and the amount of prior crystallization decrease.

The amounts of precipitated sulfides presented here have been calculated relative to the mass of the whole magma system, i.e., solids + melt (see App. 1 for details). The negative amounts shown in the sulfide precipitation diagram indicate how much sulfide with fixed composition should be added to reach sulfide saturation (Fig. 6). Sulfur content in the dry parental melt exceeds SCSS at 1,215°C, and the amount of precipitated FeCuNiS sulfides reaches 0.06 wt % at ~1,160°C (Fig. 6). Then the amount of FeCuNiS sulfide decreases to 0.02 wt % at ~1,110°C after which the amount increases close to the maximum at ~1,030°C (Fig. 6). In the parental melt with initial $H_2O$ content of 0.14 wt %, the main temperature interval for FeCuNiS sulfide precipitation is between ~965° and 1,205°C during which the mass of solids increases from

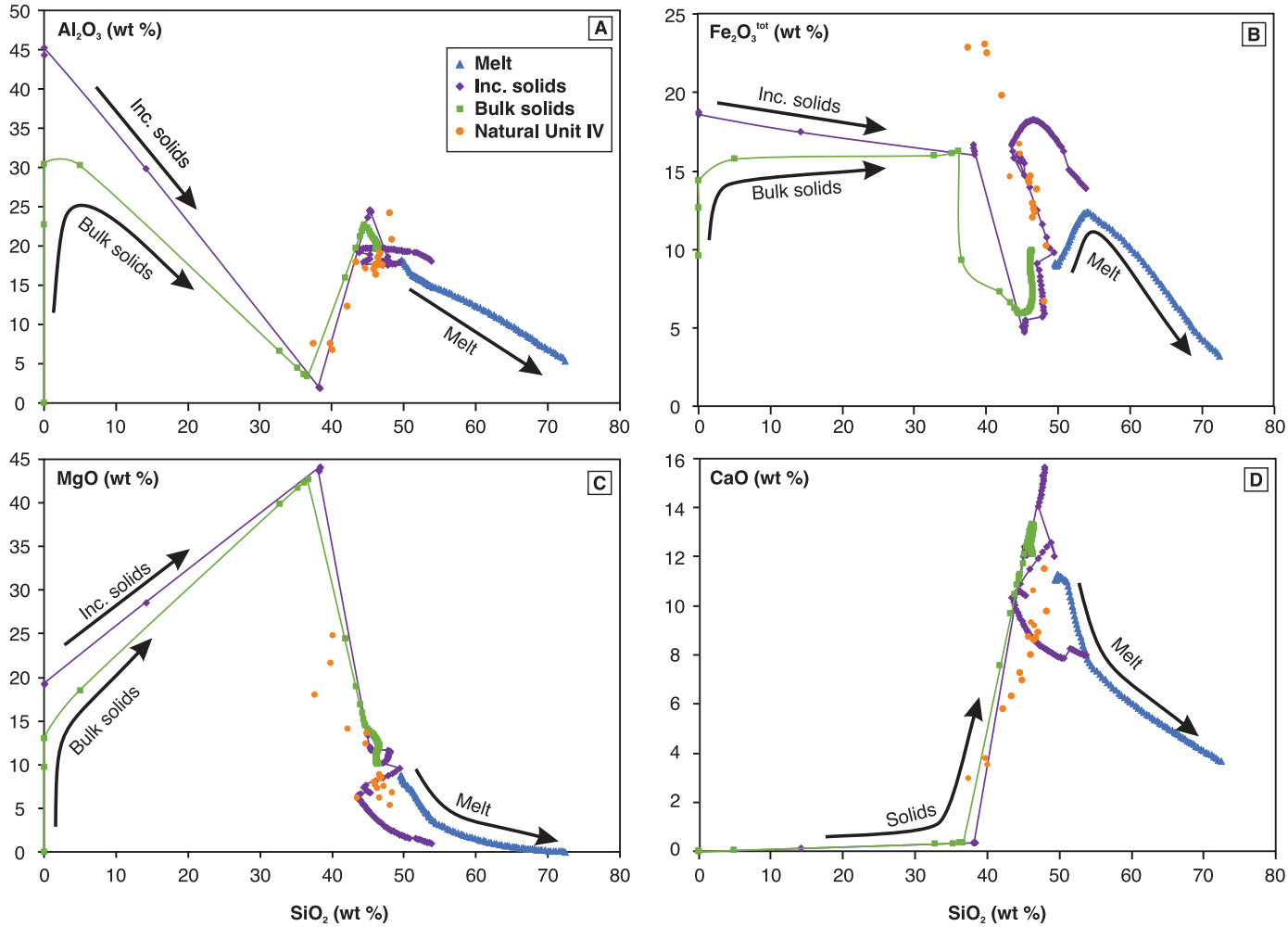


Fig. 4. (A-D) Selected solid and melt oxide compositions from the fractional crystallization simulation conducted with the parental melt containing 1 wt % $H_2O$ and initial $f_{O_2}$ at $\Delta FMQ_i$ –2 as well as from the natural cumulates from the unit IV of the Partridge River intrusion. The incremental solids indicate the composition of the solids formed within one fractionation step in the simulation, whereas the bulk composition is the summation of the previous incremental solid compositions. The data for the unit IV is from Rao and Ripley (1983), Severson (1991), and Grant and Chalokwu (1992). FMQ = fayalite-magnetite-quartz buffer.

30 to 92 m.u. (Fig. 6). When the initial $H_2O$ content of the parental melt is 1 wt %, the FeCuNiS sulfide precipitation occurs within temperature and crystal mass intervals from ~815° to 1,170°C and from 13 to 87 m.u., respectively (Fig. 6). In the simulation, where the $H_2O$ content of the parental melt is 2.25 wt %, the amount of precipitated FeCuNiS sulfide increases the most when temperature decreases from 1,145° to ~800°C while the crystallized mass increases from 3 to 83 m.u. (Fig. 6).

*Assimilation simulations*

Assimilation-fractional crystallization and SFC simulations are described for the parental melt with 1 wt % $H_2O$ and $f_{O_2}$ at $\Delta FMQ_i$ –2, because it produced the most noritic rocks in the assimilation simulations. The output of the other AFC and SFC simulations (see Fig. 2) are not described here but are available in Appendix 2. In the AFC simulation, assimilation starts when the parental melt cools from liquidus of 1,226° to 1,180°C and 5 m.u. of solids has formed (Fig. 7). Troctolite forms until the magma has assimilated 20 m.u. of wall-rock partial melt (Fig. 7). At this point, orthopyroxene replaces olivine in the $SiO_2$-rich magma, and norite forms. When the wall rock and magma reach equilibrium temperature at 1,040°C, the total amount of assimilation is 38 m.u. During the subsequent FC steps, the norite is followed early on by gabbronorite as clinopyroxene becomes stable (Fig. 7). The amount of clinopyroxene gradually decreases, however, and gabbronorite is followed by clinopyroxene-bearing norite (i.e., <5% clinopyroxene) when the magma temperature is 975°C (Fig. 7). At 855°C, olivine and clinopyroxene replace orthopyroxene in the crystallization assemblage, and augite troctolite forms until the simulation halted at 800°C (Fig. 7). The amount of residual melt is 43 m.u. at the end of the simulation (Fig. 7).

In the SFC simulations, the first stoped block is introduced when the magma temperature is 1,210°C. At this point, the initial dunite is followed by troctolite (Fig. 7). When the magma temperature reaches 1,150°C, the second stoped block is introduced. This leads to the stabilization of orthopyroxene (Fig. 7). Subsequently, olivine disappears from the crystallizing assemblage, and norite (± clinopyroxene) forms, which,

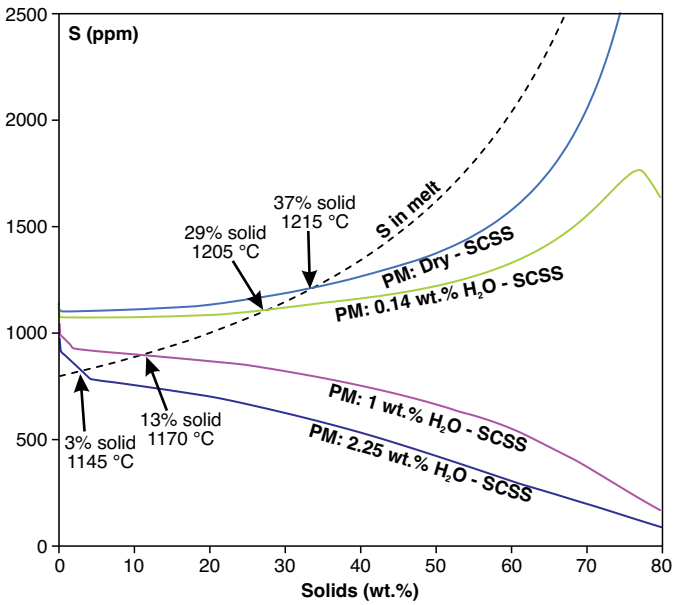


Fig. 5. The amount of solids versus sulfur content at sulfide saturation (SCSS) for the fractional crystallization simulations. The initial $f_{O_2}$ of the parental melts (PM) is $\Delta FMQ_i$ –2, and $H_2O$ contents are 0, 0.14, 1, and 2.25 wt %. The initial sulfur content of the parental melt is 800 ppm, and the amount of sulfur in the resident melt is shown with a stippled line. Sulfide saturation as well as the corresponding amount of solids and temperature of the magma are indicated with arrows for each simulation. The SCSS is calculated using the equation of Smythe et al. (2017). FMQ = fayalite-magnetite-quartz buffer.

in turn, is followed by gabbronorite (Fig. 7). When the magma temperature reaches 1,103°C, the third stoped block is added. The first rock to form is clinopyroxene-bearing norite, which is followed by gabbro during the next equilibration step (Fig. 7). In the simulation with three stoped blocks ($S_3FC$), the subsequent FC produces a rock sequence, where gabbro is followed by gabbronorite (994°C), clinopyroxene-bearing norite (974°C), troctolite (909°C), and finally augite troctolite (849°C) (Fig. 7). The amount of residual melt is 30 m.u. at the end of the model (800°C). The additional stoped block in the simulation with four stoping events ($S_4FC$) is introduced at 1,059°C, which leads to the replacement of clinopyroxene in the crystallization assemblage by orthopyroxene and consequent formation of norite (Fig. 7). Clinopyroxene becomes stable again at 1,111°C, and gabbronorite forms. The gradual decrease in modal clinopyroxene reintroduces norite (+ clinopyroxene) at 976°C, which is followed by augite troctolite at 891°C (Fig. 7). The simulation halts at 800°C, when there is 37 m.u. residual melt left.

*Sulfide saturation in the assimilation simulations*

To illustrate what controls the SCSS in the melt during assimilation, selected major element oxide concentrations in the melt (in the magma subsystem) are compared for the FC and AFC simulations with initial melt $f_{O_2}$ at $\Delta FMQ_i$ –2 and 1 wt % $H_2O$ (Fig. 8). When the assimilation of wall-rock partial melt starts in the AFC simulation, the $SiO_2$, $Al_2O_3$, $K_2O$, and $H_2O$ contents of the melt increase, whereas FeO, MgO, CaO, and $Na_2O$ contents decrease relative to the FC simulation (Fig. 8). The compositional changes in the SFC simulations are similar to the AFC simulations but less pronounced and therefore not shown here. All the observed changes in the melt composition of the AFC simulation initially decrease SCSS (Fig. 8), which makes it easier for the melt to precipitate sulfides. The first-order reason for these compositional changes is that the assimilated partial melt has higher concentrations of $SiO_2$, $Al_2O_3$, $K_2O$, and $H_2O$, which increases the concentration of these components in the melt while diluting the other oxide components. The secondary reason is that instead of crystallization of olivine and clinopyroxene, as in the FC simulation (Fig. 3), orthopyroxene crystallizes in the AFC simulation (Fig. 7). The orthopyroxene-bearing rocks in the AFC simulation are enriched in FeO compared to the rocks in the FC simulation, which leads to relative FeO depletion in the residual melt (Fig. 8) and hence decreases SCSS in the AFC simulation.

The SCSS results are shown for the AFC, $S_3FC$, and $S_4FC$ simulations in Figure 9. Melt sulfur content for AFC simulation with sulfur-free wall rock is shown to illustrate the amount of assimilated sulfur in the scenarios with different sulfur wall-rock bulk partition coefficients (Fig. 9). In the sulfur-free wall-rock scenario, the SCSS is reached when 14 m.u. of the magma has solidified and temperature is 1,140°C (Fig. 9). With wall-rock $D^{WR}$ (S) of 100, sulfide saturation occurs as the mass of solids and temperature reach 10 m.u. and 1,150°C, respectively (Fig. 9). In the AFC simulation with $D^{WR}$ (S) of 1 and 0.001, the sulfur content of the melt exceeds the SCSS when the mass of solids is ~7 m.u. and temperature is 1,150°C (Fig. 9). In the SFC simulations, the sulfide saturation occurs as the amount of solids reaches ~2 m.u. and temperature is 1,165°C. The proportions for assimilated sulfur in the melt at the end of assimilation for the different AFC are 6.1 wt % when $D^{WR}$ (S) = 100, 74.0 wt % when $D^{WR}$ (S) = 1, and 78.9 wt % when $D^{WR}$ (S) = 0.001. In the $S_3FC$ simulation, the proportion of assimilated sulfur in the melt is 69.2 wt %, and in the $S_4FC$ simulation it is 75.0 wt %.

The amount of precipitated FeCuNiS sulfide relative to the total mass of the system, i.e., solids + melt, is shown during the formation of 100 m.u. of solids and between 800° and 1,226°C (liquidus) in Figure 10. In the AFC simulation with the wall-rock $D^{WR}$ (S) = 100, the amount of precipitated sulfide in the silicate melt increases to 0.12 wt % during the AFC stage and furthermore to 0.17 wt % at 100 m.u. of solids (Fig. 10A, C). When the wall-rock $D^{WR}$ (S) is 1, the amount of precipitated FeCuNiS sulfide increases to 0.57 wt % during the AFC stage and to 0.62 wt % at 100 m.u. of solids (Fig. 10A, C). During the AFC stage of the simulation where wall-rock $D^{WR}$ (S) is 0.001, the amount of precipitated sulfide increases to 0.71 wt % and reaches 0.76 wt % when the amount of solids is 100 m.u. (Fig. 10A, C). In the $S_3FC$ simulation, the amount of immiscible FeCuNiS sulfide is 0.48 wt % at the end of stoping, and at 100 m.u. of solids the amount is 0.55 wt % (Fig. 10B, D). The fourth stoped block in the $S_4FC$ increases the amount of precipitated sulfide to 0.59 wt %, which further increases to 0.63 wt % when the solidified mass reaches 100 m.u. (Fig. 10B, D).

## Discussion

*Implications for the origin of the major rock types of the Duluth Complex*

*Formation of the Duluth Complex troctolites by fractional crystallization:* Our main objective is to study how the assimi-

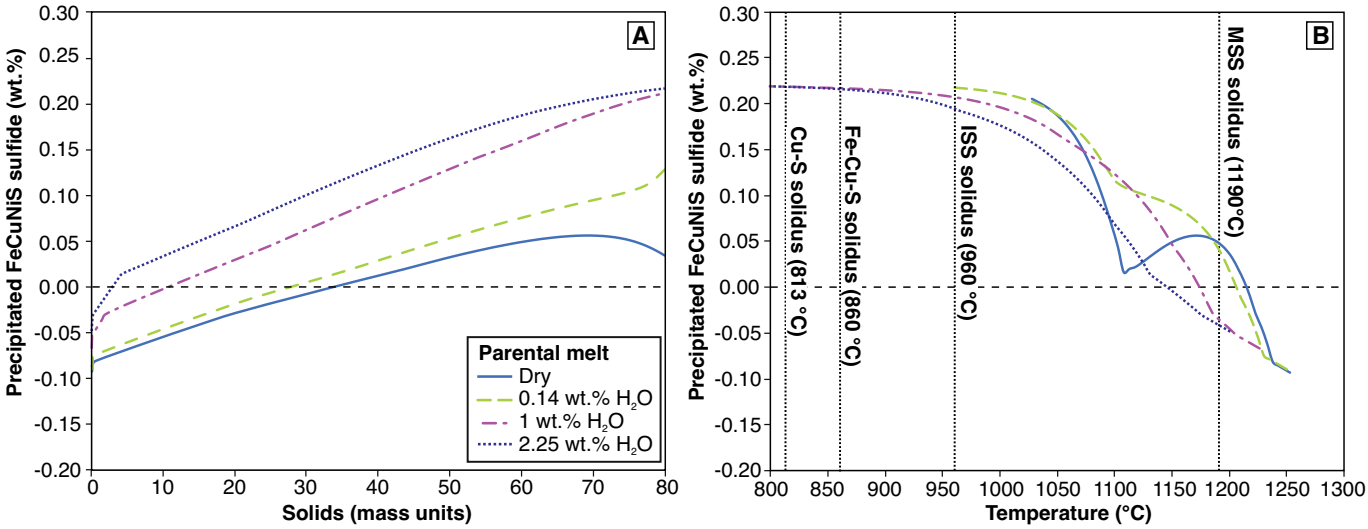


Fig. 6. Mass of solids (A) and temperature (B) of the parental magma versus the amount of sulfides (wt %) precipitated in the fractional crystallization simulations. Initial $f_{O_2}$ in the simulations is ΔFMQ –2, and the amount of sulfur in the parental melt is 800 ppm. The FeCuNiS phase approximates the average bulk sulfide content of the Duluth Complex Cu-Ni deposits (Listerud and Meineke, 1977). The amount of precipitated sulfides relative to the whole system (solids + residual melt) is calculated using the equation of Kiseeva and Wood (2015). The negative values show the degree of sulfide undersaturation with the fixed sulfide composition. The solidi for monosulfide solid solution (MSS) and intermediate solid solutions (ISS) are from Kullerud et al. (1969). FMQ = fayalite-magnetite-quartz buffer.

lation affects the SCSS, which is essentially controlled by the residual melt composition in the magma. Thus, we need to begin by discussing the controls on and patterns of the simulated residual melt compositions. To evaluate how well the simulated residual melts correspond to the natural system in the Duluth Complex, we compare the results of the FC simulations with the natural cumulates. Comparing the simulated FC rock sequences with the reference lithostratigraphy from the unit IV of the Partridge River intrusion (Severson et al., 1996) shows that none of the FC simulations perfectly match the natural rocks (Fig. 3). This is unsurprising given that (1) the composition of the parental melt is uncertain, (2) gravitational fractionation is less efficient in nature than in the simulations, and (3) equilibration with interstitial residual melt (e.g., Chalokwu et al., 1993; Ripley et al., 2007) cannot be modeled in these simulations. Also, we must acknowledge that there are uncertainties in the natural lithologies. For instance, the natural cumulate stratigraphies have mostly been constructed by visual estimates of modal mineral compositions in hand samples, which are susceptible to inaccuracies, as pointed out by Severson et al. (1996). In addition, the natural cumulates are regionally variable and include olivine gabbro and gabbro, which are absent in the reference stratigraphy but which have been reported from the Troctolitic Series in the Partridge River intrusion by many studies (e.g., Rao and Ripley, 1983; Miller and Ripley, 1996; Ripley et al., 2007; Queffurus and Barnes, 2014). Such gabbros are compatible with our FC simulations. In addition to the uncertainties mentioned above, rhyolite-MELTS is not a perfect model and relies on a limited—although large—set of experimental constraints and algorithms (e.g., Putirka, 2005; Gualda et al., 2012).

Our FC simulations show that $H_2O$ content correlates positively, and initial $f_{O_2}$ correlates negatively, with the modal olivine content (Fig. 3). The $f_{O_2}$ conditions for the formation of the Duluth Complex troctolites have been estimated to be below the FMQ buffer based on Fe-Ti oxide mineral compositions (Pasteris, 1985), which agrees with our simulations, where the most olivine-rich rocks formed with the lowest initial $f_{O_2}$ at ΔFMQ –2. In previous attempts to simulate the formation of the troctolitic rocks of Duluth Complex, crystallization was buffered at low $f_{O_2}$ conditions at ΔFMQ –2 (Ripley et al., 2007; Ripley and Li, 2013) or at Δwüstite-ilmenite +0.5 (Chalokwu et al., 1993). We decided not to buffer the crystallization conditions after the initial fixing of $FeO/Fe_2O_3$, since buffering basically requires that the melt exchanges free oxygen with its surroundings (wall rocks or cumulates), whereas unbuffered $f_{O_2}$ is controlled by the relative oxygen budgets between the crystallizing solids and the residual melt. The early and late magmatic oxides record an increase in $f_{O_2}$, from below to above the FMQ buffer, during the formation of the Duluth Complex troctolites (Pasteris, 1985), which indicates that $f_{O_2}$ was not buffered in the natural system.

Based on global data sets, mantle-derived melts, especially in continental settings, are rarely if ever completely anhydrous (e.g., Kovalenko et al., 2007; Liu, J., et al., 2017). The amount of $H_2O$ required to reach sufficient olivine stability to form extensive troctolites in our FC simulations (1–2.25 wt % $H_2O$; Fig. 3) is within the range of $H_2O$ contents (1.96 ± 1.46 wt %, $n$ = 269) suggested for intracontinental basalts on a global scale (Kovalenko et al., 2007). Based on the global comparison and because the crystallization sequence in our hydrous FC simulations (i.e., olivine → plagioclase + olivine → plagioclase + olivine + clinopyroxene ± orthopyroxene) is the same as the general cumulate sequence reported by previous studies (Miller and Ripley, 1996; Miller et al., 2002), we suggest that the parental melt of the Duluth Complex troctolites was hydrous. This interpretation is also in line with the presence of magmatic biotite in the troctolitic rocks (Weiblen and Mo-

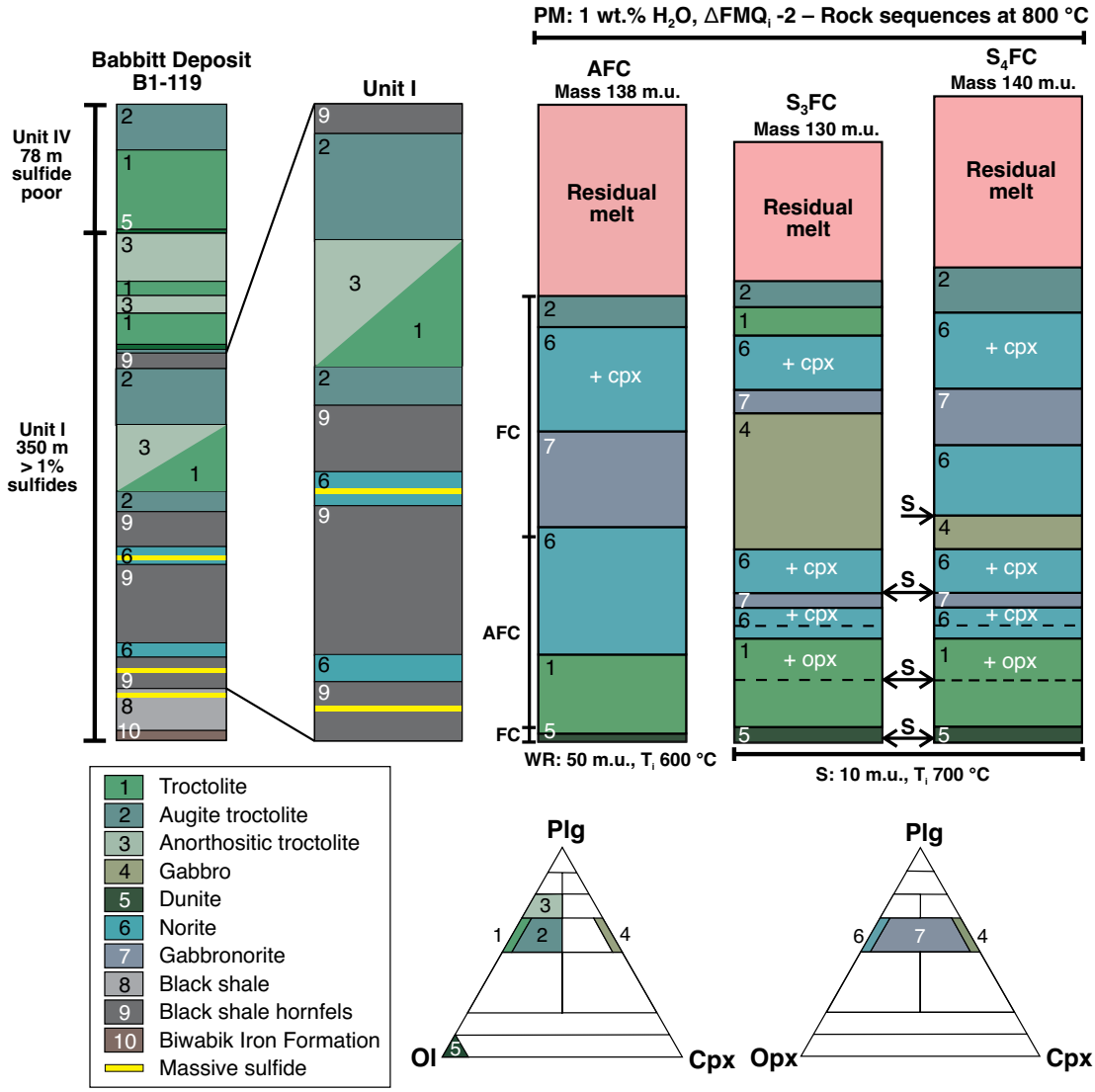


Fig. 7. The assimilation-fractional crystallization (AFC) and stoping-fractional crystallization ($S_x$FC) simulation rock sequences for the Duluth Complex parental melts at 800°C. Each stoped block in the SFC simulations is indicated with an arrow and S. The parental melt (PM) compositions in the simulations had initial $fO_2$ at $\Delta FMQ_i$ –2 and 1 wt % of $H_2O$. The total mass of the magma system is indicated above the stratigraphical columns. Simulated rock sequences were constructed with the help of the Magma Chamber Simulator Visualizer tool (Bohrson et al., 2020). The rock classification diagrams are from Phinney (1972). Abbreviations: Cpx = clinopyroxene, FMQ = fayalite-magnetite-quartz buffer, Ol = olivine, Opx = orthopyroxene, Plg = plagioclase, WR = wall rock.

rey, 1980; Saini-Eidukat et al., 1990; Ripley et al., 1993, 2007) and the local occurrence of pegmatitic troctolites (Severson and Barnes, 1991; Ripley et al., 1993; Severson et al., 1996).

In our FC simulation with the parental melt with 1 wt % $H_2O$ and $fO_2$ at ΔFMQ –2, the troctolite consists of 75 wt % of plagioclase and 25 wt % of olivine, which is well in the range of natural troctolite modal compositions with 60–80 vol % plagioclase and 10–30 vol % of olivine (Rao and Ripley, 1983; Lee and Ripley, 1996; Miller et al., 2002; Ripley et al., 2007). In the natural rocks, the primary olivine compositions were estimated to be $Fo_{56–79}$ (Chalokwu et al., 1993) and the range of measured compositions is from $Fo_{29}$ to $Fo_{71}$. In the simulation, the early olivine compositions are slightly more magnesian than the estimated primary compositions with $Fo_{85}$, and the most evolved olivine has a composition of $Fo_8$. The natural plagioclase is compositionally highly variable from $An_{35}$ to $An_{85}$ (Mainwaring and Naldrett, 1977; Rao and Ripley, 1983; Chalokwu et al., 1993; Lee and Ripley, 1996; Miller et al., 2002; Ripley et al., 2007) and closely reproduced in the simulation, where plagioclase compositions range from $An_{33}$ to $An_{85}$. Olivine gabbro and gabbro hosting 35–50 wt % clinopyroxene are major rock types in the simulation. Hence, clinopyroxene is too abundant in the simulations compared to the natural cumulates with typically ≤20 vol % of clinopyroxene, although minor cumulates with 90 vol % clinopyroxene are present locally (Rao and Ripley, 1983; Lee and Ripley, 1996; Miller et al., 2002; Ripley et al., 2007). The clinopyroxene in the simulation has Mg# from 23 to 82, which is mostly in the range of natural clinopyroxene having Mg# from 40 to 80 (Rao and Ripley, 1983; Miller et al., 2002; Ripley et al., 2007). The

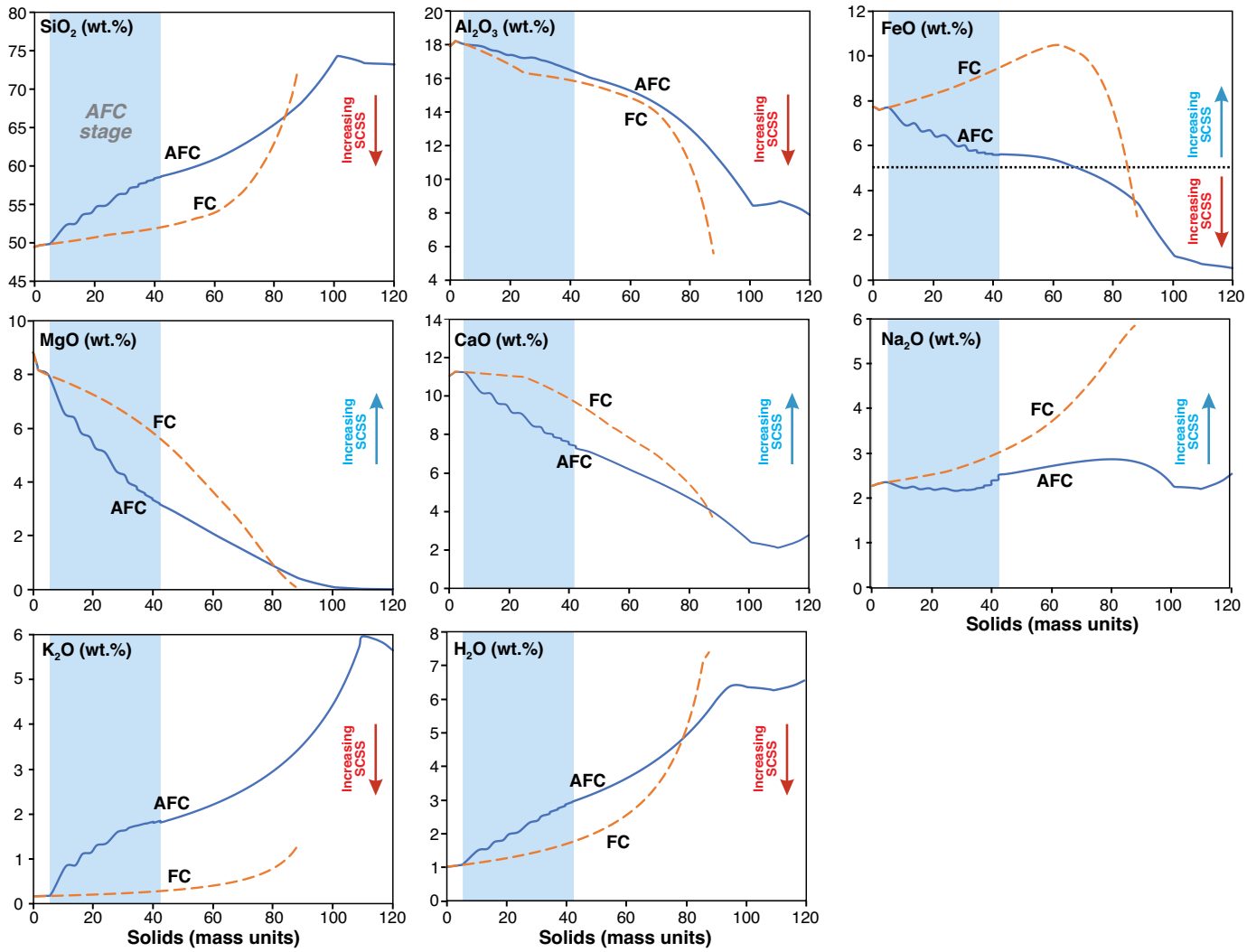


Fig. 8. Amount of solids (mass units) versus melt major element oxide contents (wt %) of the Duluth Complex parental melts with initial parental melt (PM) $H_2O$ content of 1 wt % and $f_{O_2}$ at ΔFMQ –2 in the fractional crystallization (FC; stippled line) and assimilation-fractional crystallization (AFC; solid line) simulations. The arrows qualitatively show how each oxide component affects sulfur content at sulfide saturation (SCSS) in the melt based on the SCSS model of Smythe et al. (2017). The effect of FeO on the SCSS changes from positive to negative at ~5 wt % FeO (for details, see Smythe et al., 2017). FMQ = fayalite-magnetite-quartz buffer.

most extreme simulated mineral compositions, however, represent much smaller mass of the produced crystals relative to the intermediate compositions, which are within the range of natural compositions.

The combined solid and melt compositions from the FC simulation with 1 wt % $H_2O$ and $f_{O_2}$ at $\Delta FMQ_i$ –2 are in good agreement with the natural compositions from the unit IV of the Partridge River intrusion (Fig. 4). In the case of the examined major elements, the natural compositions can be explained as mixtures of incremental solids and melt for the most part (Fig. 4). Mixtures between melt and the bulk solids are not sufficient in producing the natural compositions (Fig. 4), which implies effective crystal fractionation and accumulation. The natural cumulate compositions lie closer to the incremental solid compositions than the melt composition (Fig. 4), which implies that the amount of trapped liquid was generally small. This is compatible with the meso- and orthocumulate structures observed in the natural rocks (Chalokwu et al., 1993). The main difference between the simulations and the natural samples is that four of the most mafic natural cumulates have higher $Fe_2O_3^{tot}$ contents than any of the incremental solids from the simulation (Fig. 4). While this could result from Fe-deficient crystals forming in the simulations compared to the nature, it could also be explained by more effective gravitational accumulation of dense oxides compared to olivine in nature. In Appendix 1, Figures A2-A4, we provide similar Harker diagrams for FC simulations conducted with three other parental melts suggested for the Duluth Complex (Miller and Weiblen, 1990; Chalokwu et al., 1996; Lee and Ripley, 1996), which show that the parental melt composition used here is generally in better agreement with the natural data.

Our findings collectively suggest that the troctolitic rocks of the Duluth Complex formed via FC from parental melts, which were hydrous and initially reduced relative to the FMQ buffer. However, with 1–2.25 wt % $H_2O$, the $H_2O$/Ce of our parental

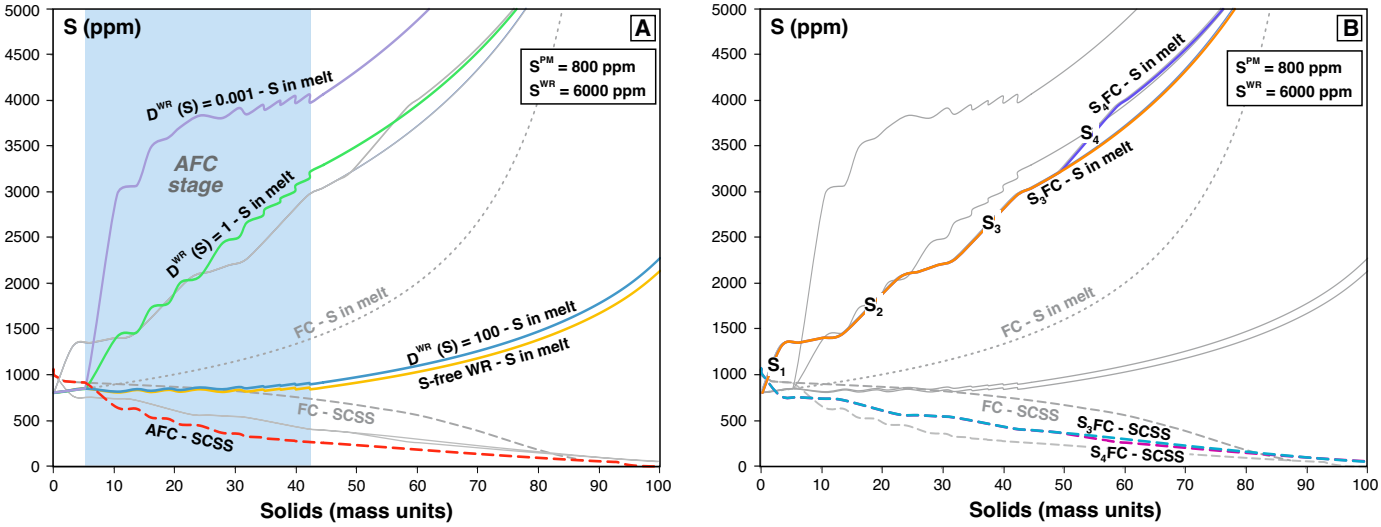


Fig. 9. The amount of solids versus sulfur content at sulfide saturation (SCSS) for the assimilation-fractional crystallization (AFC; A) and stoping-fractional crystallization (SFC; B) simulations. The initial $f_{O_2}$ of the parental melt is $\Delta FMQ_i$ –2 and $H_2O$ content is 1 wt %. $S_3FC$ stands for the simulation with three and $S_4FC$ for the simulation with four 10 mass units (m.u.) stoped blocks, and $S_x$ denotes addition of stoped blocks. The initial sulfur content is 800 ppm in the parental melt and 6,000 ppm in the wall rock. The bulk partition coefficients for sulfur [$D^{WR}$ (S)] are given for the wall-rock partial melt relative to the residual wall rock. SCSS is calculated using the equation of Smythe et al. (2017). FC = fractional crystallization, FMQ = fayalite-magnetite-quartz buffer, WR = wall rock.

magma would be 1,470–3,300 (Ce content 6.8 ppm: Basaltic Volcanism Study Project, 1981), which is in the upper range of the global compositional spectrum for intracontinental basalts (Kovalenko et al., 2007; Liu, J., et al., 2017). The high $H_2O$/Ce could either reflect anomalously Ce-poor or $H_2O$-rich mantle source or incorporation of $H_2O$ from devolatilizing wall rocks early in the magma evolution (see, e.g., Ripley, 1981; Rao and Ripley, 1983; Tyson and Chang, 1984; Saini-Eidukat et al., 1990; Thériault and Barnes, 1998; Ripley et al., 2007), which we consider a more reasonable explanation.

*Formation of the Duluth Complex norites by black shale assimilation:* In the AFC simulations, the wall-rock phase equilibrium differs from the natural system, as cordierite is not included as a phase in the MELTS algorithms. This slightly affects the composition and amount of the partial melt assimilated by the magma as a function of wall-rock temperature (further discussed in App. 1). Regardless of the differences, the presented AFC simulation has noticeable advantages over the previous binary mixing approach applied to the Duluth Complex (Ripley and Li, 2013). For the SFC scenarios with bulk assimilation, the residual wall-rock phase equilibrium is insignificant.

The AFC and SFC rock sequences of our simulations (Fig. 7) are compatible with the previous suggestions that the noritic rocks of the Partridge River intrusion in the Duluth Complex formed by assimilation of the Virginia Formation black shale (e.g., Thériault and Barnes, 1998; Ripley et al., 2007; Queffurus and Barnes, 2014; Samalens et al., 2017). In the presented AFC scenario, more norite is produced relative to the SFC scenarios (Fig. 7); this is probably because the assimilated partial melts are more $SiO_2$ rich than the bulk black shale. The implication that norite formation is more extensive with assimilation of partial melts is compatible with the widespread natural evidence of black shale partial melt assimilation in the Duluth Complex (Ripley and Alawi, 1986; Thériault and Barnes, 1998; Queffurus and Barnes, 2014; Samalens et al., 2017). The amount of assimilated black shale (~20–30 wt %) required to form the norites both in the AFC and SFC scenarios is in excellent agreement with the oxygen isotope data (Ripley et al., 2007), which indicates >20 wt % assimilation for magmas that formed the norites in the Partridge River intrusion.

### *Uncertainties in the sulfide saturation models*

Estimating the parental melt compositions for magmatic systems is subject to various uncertainties. For this reason, we have tested a range of $H_2O$ contents with the parental melt KEW-6 and three other parental melt compositions (Miller and Weiblen, 1990; Chalokwu et al., 1996; Lee and Ripley, 1996) with initial $H_2O$ contents and $f_{O_2}$ set at 1 wt % and $\Delta FMQ_i$ –2, respectively. These simulations show that, although the parental melt compositions differ considerably for several major element oxides (see App. 1, Fig. A1), the SCSS is mostly within 200 ppm, and the sulfide saturation is reached within 10 m.u. of crystallization (Fig. 11). Compared to the effects of initial $H_2O$ content (Fig. 5) and bulk sulfide composition (see below) the effect of the chosen parental melt composition on the SCSS is relatively small. The estimates for emplacement pressure of the Duluth Complex are also variable (Bonnichsen, 1975; Frost et al., 2007; Sawyer, 2014), but the wholesale effect of pressure on the phase equilibrium and hence on the SCSS is of minor importance under these conditions (Fig. 11).

To model the SCSS, we used a static sulfide composition that corresponds to the evaluated average composition of the Duluth Complex Cu-Ni deposits (Listerud and Meineke, 1977). This is a simplification and likely results in unrealistically Cu and Ni rich sulfide phase as the composition comes

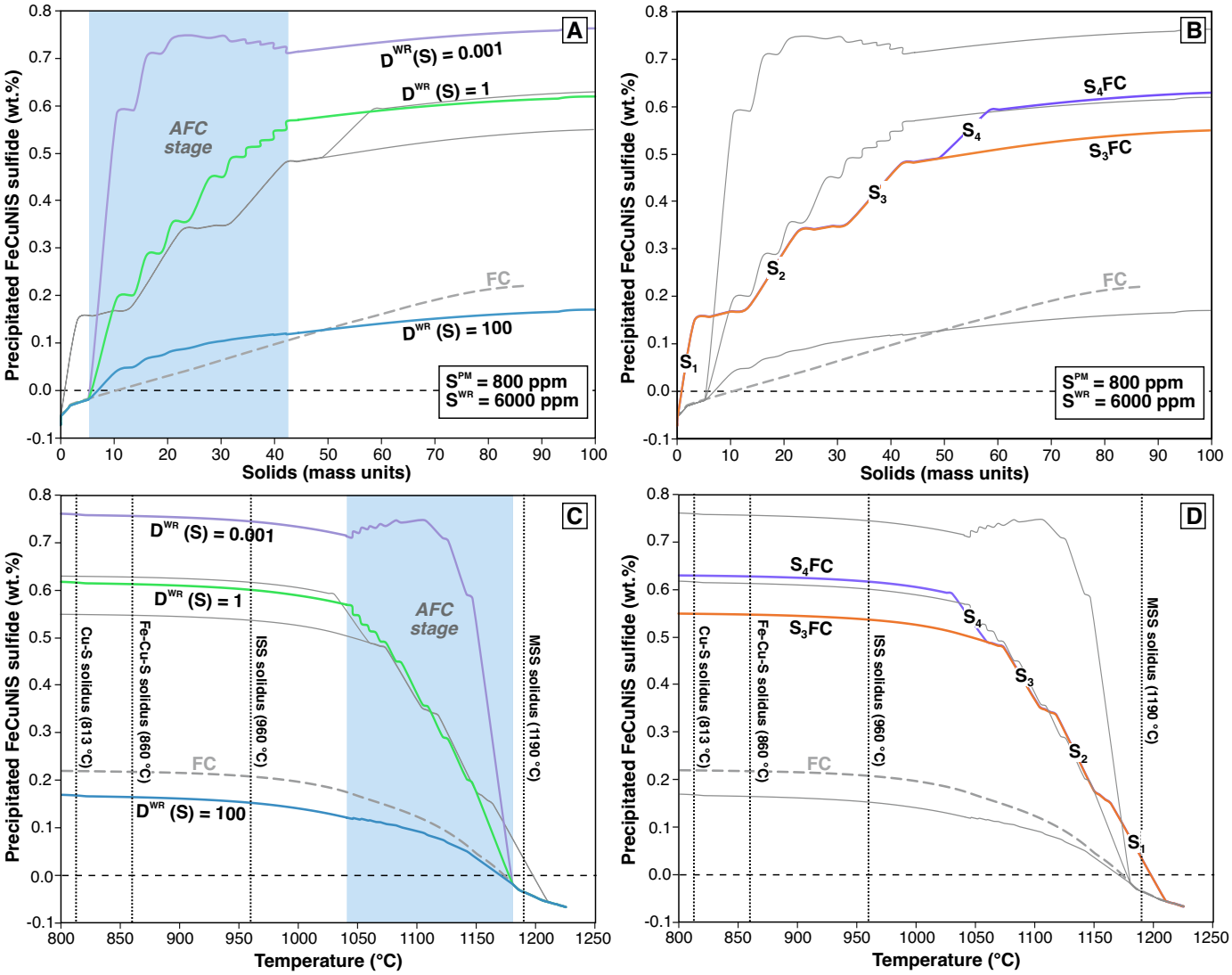


Fig. 10. Mass of solids (A, B) and temperature (C, D) of the parental magma versus the amount of precipitated sulfides (wt %) in the assimilation-fractional crystallization (AFC; A, C) and stoping-fractional crystallization (SFC; B, D) simulations. The initial $f_{O_2}$ of the parental melts is $\Delta FMQ_i$ –2, and it contains initially 1 wt % of $H_2O$. $S_3FC$ stands for the simulation with three and $S_4FC$ for the simulation with four 10 mass units (m.u.) stoped blocks, and $S_x$ denotes the addition of stoped blocks. Initial amount of sulfur in the parental melt in all of the simulations is 800 ppm and in the wall rock 6,000 ppm. The FeCuNiS phase approximates average bulk sulfide content of the Duluth Complex Cu-Ni deposits (Listerud and Meineke, 1977). The bulk partition coefficients for sulfur [$D^{WR}(S)$] are for the wall-rock partial melt relative to the residual wall rock. The amount of precipitated sulfides relative to the residual melt is calculated using the equation of Kiseeva and Wood (2015). The negative values denote the degree of undersaturation for the fixed sulfide composition. The solidi for monosulfide solid solution (MSS) and intermediate solid solutions (ISS) are from Kullerud et al. (1969). FC = fractional crystallization, FMQ = fayalite-magnetite-quartz buffer.

from the deposits, which, by definition, are enriched in these elements. As increasing Cu and Ni contents in the sulfide phase decrease SCSS (Smythe et al., 2017), our approach likely promotes early sulfide precipitation. To bracket the uncertainty related to the sulfide bulk composition, we compared the inferred FeCuNiS bulk composition with pure FeS sulfide (Fig. 11). This comparison shows that the uncertainty in the sulfide composition can shift the sulfide saturation much more dramatically than the choice of parental melt composition. A more realistic simulation would consider partitioning of Fe, Cu, and Ni in the magma and the sulfide phase(s) as well as in the wall rock in the AFC simulation. However, such a simulation would require thermodynamic sulfide phase equilibrium models, which is beyond the scope of this study.

### *The relationships of crystallization and assimilation with sulfide saturation*

*The effects of $H_2O$ on SCSS in the fractional crystallization simulations:* The previous modeling for the Duluth Complex showed that an increase in initial $H_2O$ content of the parental melt lowers the SCSS at liquidus conditions and that the SCSS decreases faster during crystallization in more hydrous

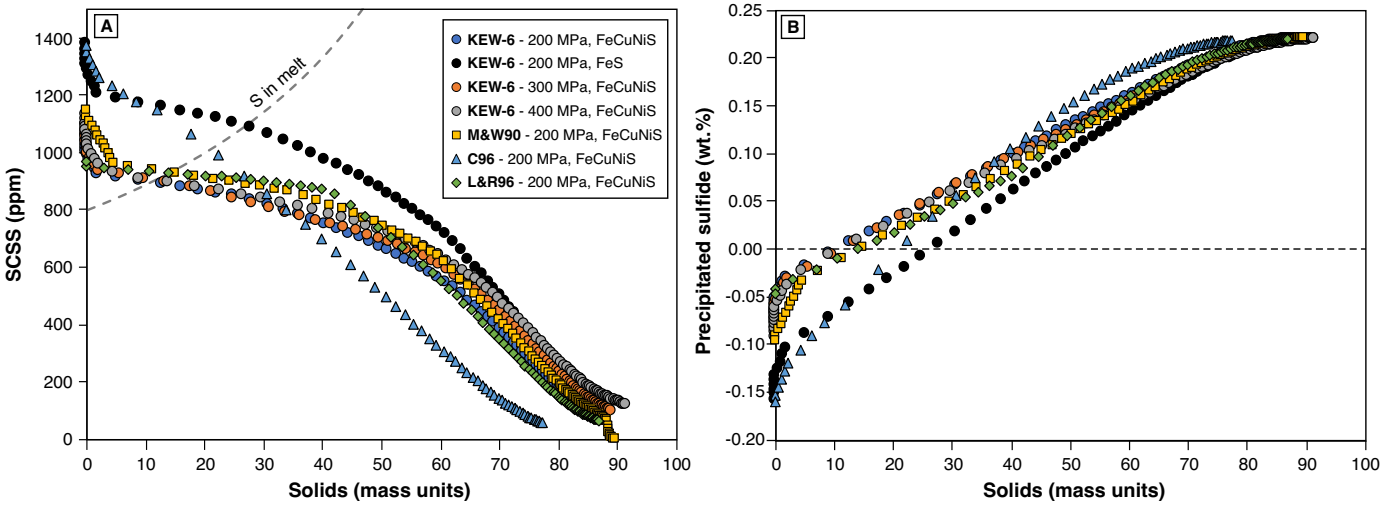


Fig. 11. Mass of solids versus sulfur content at sulfide saturation (SCSS) (A) and the amount of precipitated sulfides (B) for fractional crystallization simulations conducted with different input parameters. For the parental melt KEW-6, simulations with the FeCuNiS sulfide composition are shown at the pressures of 200, 300, and 400 MPa. For the KEW-6 at 200 MPa, the results are shown for FeS sulfide as well. The other parental melts are from Miller and Weiblen (1990; M&W90), Chalokwu et al. (1996; C96), and Lee and Ripley (1996; L&R96).

melts (Ripley and Li, 2013). The reason for the negative correlation between $H_2O$ content and SCSS was not discussed in detail, but it was suggested that possible changes in $f_{O_2}$ due to $H_2O$ addition were not of major significance (Ripley and Li, 2013). The current version of the MCS is not able to simulate continuous assimilation of fluid phase only, so we investigated the issue of added $H_2O$ by varying the $H_2O$ content of the parental melt and by assimilating $H_2O$ in the bulk stoped blocks or as a dissolved component in the wall-rock partial melts (see below).

The combined effect of higher initial $H_2O$ content in the parental magma and thus lower liquidus temperature is evident in our simulations, where the initial SCSS in the dry parental melt is 1,136 ppm, whereas in the melts with 1 and 2.25 wt % of $H_2O$ the SCSS is 1,043 and 974 ppm, respectively (Fig. 5). In addition to these first-order effects, the crystallizing phase assemblage changes as increasing $H_2O$ content (source-related or assimilated) increases olivine stability to the detriment of clinopyroxene (Fig. 3; cf. Ripley et al., 2007). This affects the liquid line of descent, most notably by lowering the FeO content and increasing the $H_2O$ content of the residual melt, which in turn considerably lowers the SCSS and thus increases sulfide stability. This pronounced second-order effect that $H_2O$ has on the liquid line of descent underlines that the qualitative first-order approximations of how the addition of certain wall-rock components (e.g., $SiO_2$, $K_2O$, or $H_2O$) affects the SCSS (Irvine, 1975; Li and Naldrett, 2000; Ripley and Li, 2013; Liu, Y., et al., 2017) can easily be oversimplified without investigating the process in terms of phase equilibria and the full set of major element oxide components.

*Effects of black shale partial melt assimilation on sulfide saturation:* Ripley and Li (2013) tested how silicate melt assimilation could have affected SCSS in the Duluth Complex parental melt by adding various amounts of generic pelite partial melt or pure $SiO_2$ to the initial parental melt composition. They concluded that selective wall-rock assimilation effectively lowers the SCSS and promotes sulfide saturation in the contaminated melt. In their simulations, sulfur was neither concentrated nor diluted by assimilation relative to the pure FC simulations.

The effects of assimilation of wall-rock partial melts on SCSS are complex, as the process involves progressive incorporation of multicomponent material to the magma (cf. Ripley and Li, 2013). In our simulations, the assimilated black shale partial melt is enriched in SCSS-decreasing oxide components ($SiO_2$, $Al_2O_3$, $K_2O$, and $H_2O$) relative to the resident melt, which leads to a gradual increase in these oxide components and consequent dilution of many of the typically SCSS-increasing oxide components (FeO, MgO, CaO, and $Na_2O$) in the resident melt (Fig. 8). All the assimilation-induced compositional changes in our simulations decrease the SCSS in the magma (Fig. 8), which should further stabilize sulfide.

Some studies have suggested that selective assimilation could decrease the SCSS and lead to increased sulfide saturation without the addition of sulfur from the wall rock (Irvine, 1975; Li and Naldrett, 2000; Seat et al., 2009; Ripley and Li, 2013). It is, however, often neglected that assimilation of sulfur-free silicate partial melt from the wall rock also leads to sulfur dilution in the magma (Fig. 9). Our simulations show that although assimilation of sulfur-free wall-rock partial melt lowers the SCSS in the magma (Fig. 9), the amount of precipitated sulfides relative to cumulate mass is only momentarily increased compared to the same magma experiencing FC, which is due to the concurrent sulfur dilution (Figs. 10, 12). The increase in early sulfide precipitation is so small that extremely effective extraction of sulfides from the concurrently crystallizing silicates would be required for economically important base metal deposits to form in such magmatic systems where sulfur-free wall rock has been assimilated.

### *Simulations with sulfur-bearing wall rock*

In the Virginia Formation contact aureole, subsolidus devolatilization fluids were considered responsible in transporting most of the assimilated sulfur to the troctolite-hosted deposits

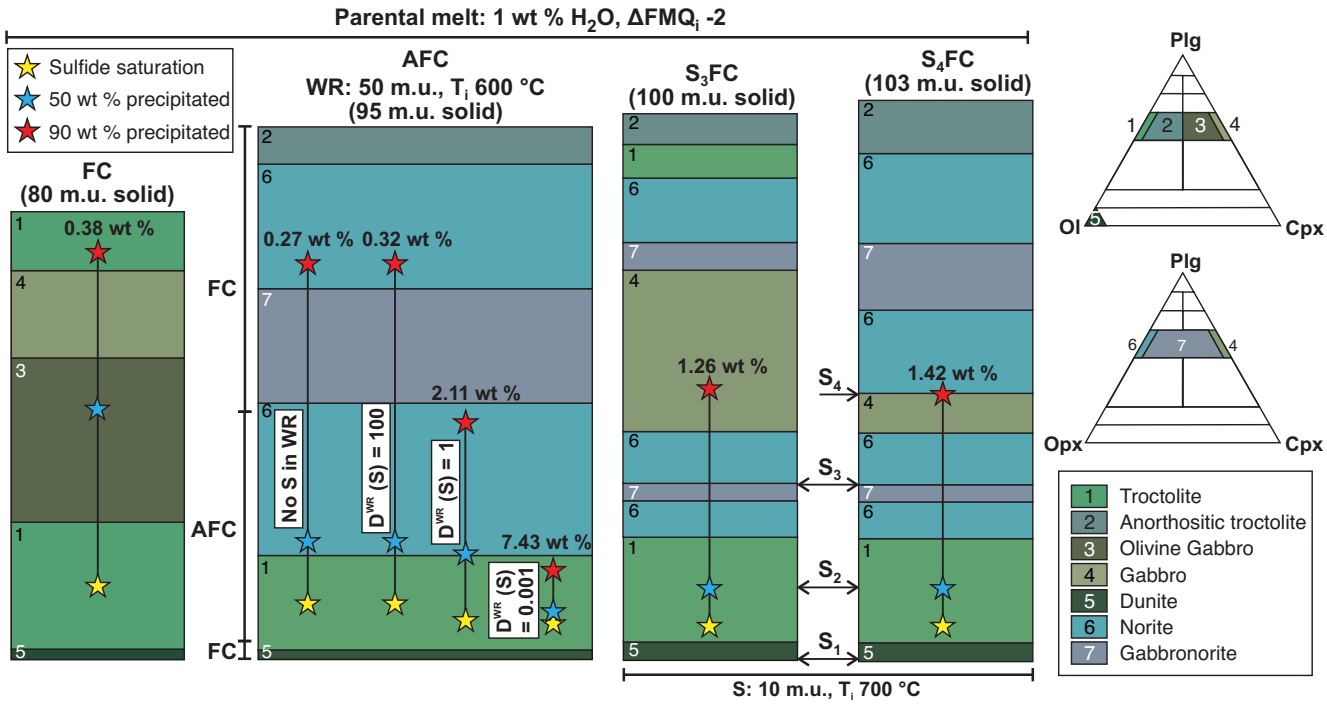


Fig. 12. Simulated rock sequences (by mass) for the representative fractional crystallization (FC), assimilation-fractional crystallization (AFC), and stoping-fractional crystallization (SFC) simulations. The stars indicate sulfide saturation (yellow) as well as 50 wt % (blue) and 90 wt % (red) precipitated sulfides relative to the total mass of sulfides produced by the respective simulations. The numbers in wt % above red stars indicate average sulfide content through the rocks from sulfide saturation to 90 wt % precipitated sulfides, i.e., between the yellow and red stars. For the AFC rock sequence, simulations with sulfur-free wall rock (WR) and sulfur-bearing wall rock with $D^{WR}$ (S) = 100, 1, and 0.001 are shown. The initial sulfur content of the magma is 800 ppm for all the simulations, and wall-rock sulfur content is 6,000 ppm in the AFC and SFC simulations. Cpx = clinopyroxene, FC = fractional crystallization, FMQ = fayalite-magnetite-quartz buffer, Ol = olivine, Opx = orthopyroxene, Plg = plagioclase.

(Ripley, 1981; Rao and Ripley, 1983; Tyson and Chang, 1984; Thériault and Barnes, 1998; Ripley et al., 2007). The norite-hosted deposits were suggested to form when black shale partial melts transported sedimentary sulfides (either solid or molten) to the magma (Thériault and Barnes, 1998; Queffurus and Barnes, 2014; Samalens et al., 2017). Sulfur mobility and transportation from the wall rock to the magma depends on several factors, including sulfide phase equilibrium, reaction kinetics and the ability of fluid or partial melt to migrate toward the magma. All these processes are currently poorly known, which hampers simulating selective sulfur assimilation. We treated sulfur as a trace element with different partition coefficients as a proxy for the different modes of sulfur mobilization and transportation introduced above. We tentatively use these data to discuss the sulfur assimilation and formation of the troctolite and norite-hosted Cu-Ni deposits of the Duluth Complex. Ripley (1981) suggested that ~75 wt % of the sulfur within the troctolitic Dunka Road Cu-Ni deposit of the Partridge River intrusion was derived from the Virginia Formation black shale, which we adopt as a target value for assimilated sulfur. Sulfur isotope composition in the norite-hosted Cu-Ni deposits at the Babbitt deposit of the Partridge River intrusion shows a similar affinity to the Virginia Formation black shale (Arcuri et al., 1998).

The simulation where sulfur is highly compatible with the wall-rock residual [$D^{WR}$ (S) = 100; Figs. 9, 10] is a proxy for the scenario where sulfurous fluid in the black shale reacts with Fe-bearing minerals and forms additional pyrrhotite as suggested by, e.g., Andrews and Ripley (1989) and Arcuri et al. (1998). Pyrrhotite has a high melting point at ~1,190°C (Kullerud et al., 1969); hence, in this scenario only a minor amount of sulfur, mostly in the form of solid pyrrhotite, gets transported to the magma via silicate partial melt. In our simulation, the largest proportion for black shale-derived sulfur in the melt is ~6 wt % of the total sulfur, which is not compatible with the isotopic criteria (Ripley, 1981). In this scenario, nearly wholesale melting of the black shale would be required to supply the magma with enough sulfur. Hence, we consider this scenario unlikely for the formation of the Cu-Ni deposits of the Duluth Complex if selective assimilation of partial melts dominated over bulk assimilation.

In the AFC simulation where sulfur is highly incompatible to the black shale residual [$D^{WR}$ (S) = 0.001; Figs. 9, 10], nearly all the wall-rock sulfur gets assimilated in the early stage. In this simulation, sulfur partitions from the wall rock to the partial melt, but the amount of sulfur assimilated is orders of magnitude larger than can realistically be dissolved. As fluid assimilation at subsolidus conditions cannot be currently modeled with the MCS, we intend this scenario as a tentative proxy for the early release of sulfur by wall-rock devolatilization fluids (Ripley, 1981; Thériault and Barnes, 1998; Ripley et al., 2007). Since sulfur mobilization via devolatilization can occur already at ~400°C (Ripley, 1981; Rao and Ripley, 1983), it could take place possibly without any partial melt

assimilation and from a larger volume of wall-rock material than considered in our simulations. Hence, the overly incompatible sulfur partition coefficient of $D^{WR}$ (S) of 0.001 might not exaggerate the overall sulfur mass balance. In this AFC simulation black shale contributes ~79 wt % of sulfur in the magma, and ~90 wt % of the sulfides precipitate during the formation of early troctolitic rocks (Fig. 12). These results are in excellent agreement with the proposed fluid assimilation for the troctolitic Cu-Ni deposits (Ripley, 1981; Rao and Ripley, 1983; Tyson and Chang, 1984; Thériault and Barnes, 1998; Ripley et al., 2007).

In the intermediate case with sulfur equally compatible with the partial melt and residual black shale (Figs. 9, 10), the amount of assimilated sulfur is again much higher than what could realistically dissolve into the wall-rock partial melt. This simulation is intended as a proxy for a scenario where half of the solid or molten sulfides get selectively transported to the magma via partial melt assimilated from the black shale footwall and xenoliths (see Queffurus and Barnes, 2014; Samalens et al., 2017). The proportion of black shale sulfur in the magma increases to 74 wt % in the simulation, which is compatible with the sulfur isotope data (Ripley, 1981). Furthermore, ~50 wt % of sulfide precipitation takes place during troctolite formation and ~40 wt % during the subsequent norite formation (Fig. 12), which complies with the suggestion that selective sulfide extraction from the black shale via assimilated partial melts (Thériault and Barnes, 1998; Queffurus and Barnes, 2014; Samalens et al., 2017) is a suitable process for the formation of both troctolite- and norite-hosted Cu-Ni deposits of the Duluth Complex.

The SFC simulations correspond to a case where xenoliths are fully digested by the magma (by melting and/or dissolution). In the $S_3$FC simulation, the wall-rock sulfur proportion in the melt is 69.2 wt % and in the $S_4$FC simulation 75.0 wt %. Hence, bulk assimilation of stoped xenoliths is also, in theory, a possible mechanism for sulfide assimilation for the norite-hosted Cu-Ni deposits, but not for the troctolites. Xenoliths are a considerable heat sink, however, especially if their temperatures are well below their solidi. The introduction of the second, third, and fourth stoped block in our simulations results in almost equal mass of crystallization in the magma. In addition, the 10-m.u. portions of wall-rock material used in the simulation should each be composed of numerous small xenoliths with large surface versus volume ratio for the consequences predicted by thermodynamics to be effective.

### *Implications on sulfide saturation and formation of Cu-Ni deposits in the Duluth Complex*

Unit IV of the Partridge River intrusion, which likely formed via FC, is variably sulfide bearing with 0.01–0.21 wt % S (Ripley and Alawi, 1986; Severson, 1991; Ripley et al., 2007), but the distribution and composition of the sulfides are poorly defined, which makes comparison to our FC sulfide saturation models difficult. Hence, we concentrate on the sulfide precipitation in the AFC and SFC simulations. In these simulations, sulfide precipitation mostly occurs at temperatures between the monosulfide solid solution (MSS) and intermediate solid solution (ISS) solidi (Fig. 10C). The Cu content of the inferred bulk sulfide phase (47.8 wt % Fe, 12.2 wt % Cu, 3.9 wt % Ni, and 36.1 wt % S) is higher than what can be incorporated in MSS (~5 wt %; Kullerud et al., 1969), which implies coprecipitation of MSS and Cu-rich sulfide melt. The simulations are compatible with the previous studies, which attribute the formation of the Duluth Complex Cu-Ni deposits to coprecipitation of MSS and immiscible Cu-rich sulfide melt, of which the latter gravitationally accumulates and fractionally crystallizes to additional MSS and ISS (Rao and Ripley, 1983; Thériault and Barnes, 1998; Queffurus and Barnes, 2014; Samalens et al., 2017). The relative proportions of molten and solid sulfides and subsequent fractional crystallization of the sulfide melt, however, cannot be evaluated without thermodynamic modeling of the sulfide system. Knowledge of the sulfide melt proportion would be essential for studying base metal and PGE partitioning between silicate and sulfide systems, since these elements partition differently to MSS and sulfide melt in general (e.g., Fleet et al., 1993; Li and Audétat, 2012). Here we shortly discuss the timing and degree of sulfide precipitation as well as the role of dynamic sulfide accumulation in the light of presented AFC and SFC simulations.

Firstly, we use the average sulfur content of the Duluth Complex Cu-Ni deposits, 2.64 wt % (Listerud and Meineke, 1977), and our suggested FeCuNiS bulk sulfide composition (47.8 wt % Fe, 12.2 wt % Cu, 3.9 wt % Ni, and 36.1 wt % S) to estimate that the deposits contain ~7.3 wt % of sulfides on average. The thicknesses of the deposits are highly variable (15–335 m), but their shapes and sizes relative to those of the whole intrusion were not estimated by Listerud and Meineke (1977). Hence, we only compare the sulfide contents and the hosting rock types between the natural settings and the simulations. The simulated average sulfide contents have been calculated relative to the solids formed from the moment of sulfide saturation and until 90 wt % of the total sulfides have precipitated, i.e., between the yellow and red stars in Figure 12. This approach assumes that silicates, oxides, and sulfides accumulate with equal efficiency.

In the AFC simulations with sulfur-free wall rock and $D^{WR}$ (S) of 100, the timing and degree of sulfide precipitation are nearly identical with 50 wt % of the sulfides precipitated (relative to the maximum amount at the end of the simulation) at the early stage of norite formation (~20 m.u. solid) and 90 wt % of sulfides have precipitated, when 70 m.u. of solids have formed (Fig. 12). Compared to the FC simulation, the amount of precipitated sulfides is slightly increased early in the AFC stage, but when the AFC system has precipitated 90 wt % of sulfides, the average sulfide content of the cocrystallized rocks is smaller (0.27–0.32 wt %) compared to the FC simulation (0.38 wt %) (Fig. 12). With such low sulfide concentrations, these simulations are highly unlikely to form economically important sulfide deposits, unless the dynamic upgrading by physical processes is extremely efficient.

In the AFC simulations with $D^{WR}$ (S) = 0.001, 90 wt % of sulfides precipitate already within the early troctolite formation stage, where the resulting average sulfide content is 7.43 wt % (Fig. 12), which is nearly identical to the inferred natural average sulfide content of ~7.3 wt %. This implies that where the black shale sulfur can be efficiently mobilized and transported to the magma, dynamic upgrading may be of secondary importance in generating economically important sulfide deposits. In the simulation, where $D^{WR}$ (S) is 1, ~50 wt % of the sulfides precipitate during troctolite formation

and the system reaches 90 wt % sulfide precipitation during the subsequent norite formation (Fig. 12). The average sulfide content within the coprecipitating solids is 2.11 wt % (Fig. 12), which is less than in the inferred ~7.3 wt % sulfides in the natural deposits. In the $S_3$FC and $S_4$FC simulations, the cumulate portions, within which 90 wt % of sulfide precipitation occurs, have average sulfide contents of 1.26 and 1.42 wt %, respectively (Fig. 12). These contents are lower than in the AFC simulations with $D^{WR}$ (S) ≤ 1, which means that more effective dynamic upgrading is required to form economically important deposits if bulk assimilation is the dominant assimilation process. Bulk assimilation also requires more crystallization in the magma compared to AFC, which hinders the dynamic sulfide upgrading by an efficient flow of magma or gravitational settling through the silicate cumulates. In the Duluth Complex, where the Cu-Ni deposits are present at the proximity of devolatilized and partially molten black shale footwall and xenoliths (Rao and Ripley, 1983; Ripley and Alawi, 1986; Thériault and Barnes, 1998; Queffurus and Barnes, 2014; Samalens et al., 2017), we suggest that AFC, i.e., selective assimilation of fluids and partial melts, is the dominant mode of sulfur assimilation, whereas bulk assimilation is likely of lesser importance.

## Conclusions

The presented MCS simulations aid interpretations of the observed natural cumulate sequences in the contact zone of the Partridge River intrusion of the Duluth Complex that formed via fractional crystallization and assimilation processes. The troctolites are likely formed via fractional crystallization of hydrous (≥1 wt % $H_2O$) parental melt, whereas formation of norites requires ~20–30 wt % assimilation of Virginia Formation black shale. Both the AFC simulation with progressive assimilation of partial melt and the bulk assimilation model with stoped blocks are sufficient formation processes for the norites, although the norites form more extensively in the AFC simulation.

Our results show that $H_2O$, whether source related or assimilated, lowers SCSS in the magma both directly and indirectly. In the latter case, olivine stability, which is increased by higher $H_2O$ content, decreases FeO in the residual melt, thus lowering SCSS. Assimilation of black shale partial melt can also lower SCSS in the magma, but if the assimilated portion is sulfur poor, sulfide saturation is only moderately increased during assimilation compared to FC, as suggested by our sulfur trace element simulation, where sulfur is compatible in black shale wall rock during assimilation [$D^{WR}$ (S) = 100]. With moderate mobility [$D^{WR}$ (S) = 1] dynamic sulfide accumulation still needs to be efficient to form economically important deposits, but if sulfur is efficiently mobilized and transported to the magma via devolatilization fluids, the role of dynamic accumulation may be of lesser importance. Bulk assimilation can also supply the magma with considerable amounts of black shale sulfur, but it is considered less likely to be the dominant assimilation process, as it should be accompanied by more efficient dynamic sulfide upgrading in more crystalline magma.

Even though there certainly is room for improvement in the presented thermodynamic + geochemical models—for example, related to considerations of devolatilization, phase equilibria of the wall rock, and kinetic factors—comparison to the natural rocks from the Duluth Complex is encouraging and suggests that the MCS is a useful tool in studying SCSS and effects of assimilation in open magmatic systems. This work provides a more nuanced and complete understanding of how magma interaction with country rock can modulate the sulfur and metal content of magmas, particularly as compared to classic binary mixing or bulk assimilation models. Critically, this work highlights how the MCS can be used to help understand sulfide precipitation in ore-forming systems and potentially to predict sulfur emissions from open systems in modern and extinct volcanic settings. Going forward, studies of chalcophile metals in ancient and modern settings would benefit from considering how AFC and SFC might modulate sulfide and metal availability, especially as many recent studies have highlighted the importance of early Fe loss (Barber et al., 2021), magmatic $H_2O$ (Rezeau and Jagoutz, 2020), and sulfur degassing (Wieser et al., 2020) on the metal budgets in active and ore-forming volcanic systems.

## Acknowledgments

We thank Maria Emilia Schutesky for handling the editorial process. Giada Iacono-Marziano and an anonymous reviewer are thanked for their constructive reviews and Fabio Cafagna for helpful discussions. V.J.V. and J.S.H. are funded by the Academy of Finland grants 295129, 306962, and 327358.

## REFERENCES

Andrews, M.S., and Ripley, E.M., 1989, Mass transfer and sulphur fixation in the contact aureole of the Duluth Complex: The Canadian Mineralogist, v. 27, p. 293–310.

Arcuri, T., Ripley, E.M., and Hauck, S.A., 1998, Sulphur and oxygen isotope studies of the interaction between pelitic xenoliths and basaltic magma at the Babbitt and Serpentine Cu-Ni deposits, Duluth Complex, Minnesota: Economic Geology, v. 93, p. 1063–1075.

Barber, N.D., Edmonds, M., Jenner, F., Audétat, A., and Williams, H., 2021, Amphibole control on copper systematics in arcs: Insights from the analysis of global datasets: Geochimica et Cosmochimica Acta, v. 307, p. 192–211.

Barnes, S.J., Cruden, A.R., Arndt, N., and Saumur, B.M., 2016, The mineral system approach to magmatic Ni-Cu-PGE sulphide deposits: Ore Geology Reviews, v. 76, p. 296–316.

Basaltic Volcanism Study Project, 1981, Basaltic volcanism on the terrestrial planets: New York, Pergamon Press, p. 30–77.

Benkó, Z., Mogessie, A., Molnár, F., Krenn, K., Poulson, S.R., Hauck, S., Severson, M., and Arehart, G.B., 2015, Hydrothermal alteration and Ni-Cu-PGE mobilization in the charnockitic rocks of the footwall of the South Kawishiwi intrusion, Duluth Complex, USA: Ore Geology Reviews, v. 67, p. 170–188.

Benkó, Z., Mogessie, A., Molnár, F., Hauck, S.A., Severson, M.J., and Ettinger, K., 2018, The influence of thermal differences and variation of Cl-F-OH ratios on Cu-Ni-PGE mineralization in the contact aureole of the South Kawishiwi intrusion, Duluth Complex: Geosciences, v. 8, p. 1–35.

Bohrson, W.A., Spera, F.J., Ghiorson, M.S., Brown, G.A., Creamer, J.B., and Mayfield, A., 2014, Thermodynamic model for energy-constrained open-system evolution of crustal magma bodies undergoing simultaneous recharge, assimilation and crystallization: the Magma Chamber Simulator: Journal of Petrology, v. 55, p. 1685–1717.

Bohrson, W.A., Spera, F.J., Heinonen, J.S., Brown, G.A., Scruggs, M.A., Adams, J.V., Takach, M.K., Zeff, G., and Suikkanen, P.E., 2020, Diagnosing open-system magmatic processes using the Magma Chamber Simulator (MCS): Part I—major elements and phase equilibria: Contributions to Mineralogy and Petrology, v. 175, p. 1–29.

Bonnichsen, B., 1975, Geology of the Biwabik iron formation, Dunka River area, Minnesota: Economic Geology, v. 70, p. 319–340.

Chalokwu, C.I., Grant, N.K., Ariskin, A.A., and Barmina, G.S., 1993, Simulation of primary phase relations and mineral compositions in the Partridge

River intrusion, Duluth Complex, Minnesota: Implications for the parent magma composition: Contributions to Mineralogy and Petrology, v. 114, p. 539–549.

Chalokwu, C.I., Ariskin, A.A., and Koptev-Dornikov, E.V., 1996, Magma dynamics at the base of an evolving magma chamber: Incompatible element evidence from the Partridge River intrusion, Duluth Complex, Minnesota, USA: Geochimica et Cosmochimica Acta, v. 60, p. 4997–5011.

Fleet, M.E., Chryssoulis, S.L., Stone, W.E., and Weisener, C.G., 1993, Partitioning of platinum-group elements and Au in the Fe-Ni-Cu-S system: Experiments on the fractional crystallization of sulfide melt: Contributions to Mineralogy and Petrology, v. 115, p. 36–44.

Fortin, M.-A., Riddle, J., Desjardins-Langlais, Y., and Baker, D.R., 2015, The effect of water on the sulfur concentration at sulfide saturation (SCSS) in natural melts: Geochimica et Cosmochimica Acta, v. 160, p. 100–116.

Frost, C.D., von Blanckenburg, F., Schoenberg, R., Frost, B.R., and Swapp, S.M., 2007, Preservation of Fe isotope heterogeneities during diagenesis and metamorphism of banded iron formation: Contributions to Mineralogy and Petrology, v. 153, p. 211–235.

Ghiorso, M.S., and Gualda, G.A.R., 2015, An $H_2O$-$CO_2$ mixed fluid saturation model compatible with rhyolite-MELTS: Contributions to Mineralogy and Petrology, v. 169, p. 1–30.

Ghiorso, M.S., and Sack, R.O., 1995, Chemical mass transfer in magmatic processes IV. A revised and internally consistent thermodynamic model for the interpolation and extrapolation of liquid-solid equilibria in magmatic systems at elevated temperatures and pressures: Contributions to Mineralogy and Petrology, v. 119, p. 197–202.

Grant, N.K., and Chalokwu, C.I., 1992, Petrology of the Partridge River intrusion, Duluth Complex, Minnesota: II. Geochemistry and strontium isotope systematics in drill core DDH-221: Journal of Petrology, v. 33, p. 1007–1038.

Grant, N.K., and Molling, P.A., 1981, A strontium isotope and trace element profile through the Partridge River troctolite, Duluth Complex, Minnesota: Contributions to Mineralogy and Petrology, v. 77, p. 296–305.

Gualda, G.A.R., Ghiorso, M.S., Lemons, R.V., and Carley, T.L., 2012, Rhyolite-MELTS: A modified calibration of MELTS optimized for silica-rich, fluid-bearing magmatic systems: Journal of Petrology, v. 53, p. 875–890.

Heinonen, J.S., Bohrson, W.A., Spera, F.J., Brown, G.A., Scruggs, M.A., and Adams, J.V., 2020, Diagnosing open-system magmatic process using the Magma Chamber Simulator (MCS): Part II—trace elements and isotopes: Contributions to Mineralogy and Petrology, v. 175, p. 1–21.

Heinonen, J.S., Iles, K.A., Heinonen, A., Fred, R., Virtanen, V.J., Bohrson, W.A., and Spera, F.J., 2021, From binary mixing to Magma Chamber Simulator—geochemical modeling of assimilation in magmatic systems, *in* Masotta, M., Beier, C., and Mollo, S., eds., Crustal magmatic systems: Anatomy, architecture, and physico-chemical processes: New Jersey, Wiley, p. 151–176.

Holness, M.B., and Sawyer, E.W., 2008, On the pseudomorphing of melt-filled pores during the crystallization of migmatites: Journal of Petrology, v. 49, p. 1343–1363.

Iacono-Marziano, G., Ferraina, C., Gaillard, F., Di Carlo, I., and Arndt, N.T., 2017, Assimilation of sulfate and carbonaceous rocks: Experimental study, thermodynamic modeling and application to the Noril'sk-Talnakh region (Russia): Ore Geology Reviews, v. 90, p. 399–413.

Irvine, T.N., 1975, Crystallization sequences in the Muskox intrusion and other layered intrusions—II. Origin of chromitite layers and similar deposits of other magmatic ores: Geochimica et Cosmochimica Acta, v. 39, p. 991–1020.

Jugo, P.J., Wilke, M., and Botcharnikov, R.E., 2010, Sulfur K-edge XANES analysis of natural and synthetic basaltic glasses: Implications for S speciation and S content as a function oxygen fugacity: Geochimica et Cosmochimica Acta, v. 74, p. 5926–5938.

Kiseeva, E.S., and Wood, B.J., 2015, The effects of composition and temperature on chalcophile and lithophile element partitioning into magmatic sulphides: Earth and Planetary Science Letters, v. 424, p. 280–294.

Kovalenko, V.I., Naumov, V.B., Girnis, A.V., Dorofeeva, V.A., and Yarmolyuk, V.V., 2007, Average compositions of magmas and mantle sources of mid-ocean ridges and intraplate oceanic and continental settings estimated from the data on melt inclusions and quenched glasses of basalts: Petrology, v. 15, p. 361–396.

Kullerud, G., Yund, R.A., and Moh, G.H., 1969, Phase relation in the Cu-Fe-S, Cu-Ni-S, and Fe-Ni-S systems: Economic Geology Monograph 4, p. 323–343.

Lee, I., and Ripley, E.M., 1996, Mineralogic and oxygen isotopic studies of open system magmatic processes in the South Kawishiwi intrusion, Spruce Road area, Duluth Complex, Minnesota: Journal of Petrology, v. 37, p. 1437–1461.

Lesher, C.M., 2019, Up, down, or sideways: Emplacement of magmatic Fe-Ni-Cu-PGE sulfide melts in large igneous provinces: Canadian Journal of Earth Sciences, v. 56, p. 756–773.

Li, C., and Naldrett, A.J., 2000, Melting reactions of gneissic inclusions with enclosing magma at Voisey's Bay, Labrador, Canada: Implications with respect to ore genesis: Economic Geology, v. 95, p. 801–814.

Li, C., and Ripley, E.M., 2009, Sulfur contents at sulfide-liquid or anhydrite saturation in silicate melts: Empirical equations and example applications: Economic Geology, v. 104, p. 405–412.

Li, Y., and Audétat, A., 2012, Partitioning of V, Mn, Co, Ni, Cu, Zn, As, Mo, Ag, Sn, Sb, W, Au, Pb, and Bi between sulfide phases and hydrous basanite melt at upper mantle conditions: Earth and Planetary Science Letters, v. 355–356, p. 327–340.

Listerud, W.H., and Meineke, D.G., 1977, Mineral resources of a portion of the Duluth Complex and adjacent rocks in St. Louis and Lake Counties, northeastern Minnesota: Minnesota Department of Natural Resources Division of Minerals, Report 93, p. 1–84.

Liu, J., Xia, Q.-K., Kuritani, T., Hanski, E., and Yu, H.-R., 2017, Mantle hydration and the role of water in the generation of large igneous provinces: Nature Communications, v. 8, p. 1–8.

Liu, Y., Samaha, N.-T., and Baker, D.R., 2007, Sulfur concentration at sulfide saturation (SCSS) in magmatic silicate melts: Geochimica et Cosmochimica Acta, v. 71, p. 1783–1799.

Liu, Y., Li, W., Lü, X., Liu, Y., Ruan, B., and Liu, X., 2017, Sulfide saturation mechanism of Poyi magmatic Cu-Ni sulfide deposit in Beishan, Xinjian, Northwest China: Ore Geology Reviews, v. 91, p. 419–431.

Mainwaring, P.R., and Naldrett, A.J., 1977, Country-rock assimilation and the genesis of Cu-Ni sulfides in the Water Hen intrusion, Duluth Complex, Minnesota: Economic Geology, v. 72, p. 1269–1284.

Miller, J.D., Jr., and Ripley, E.M., 1996, Layered intrusions of the Duluth Complex, Minnesota, USA, *in* Cawthorn, R.G., ed., Layered intrusions: Amsterdam, Netherlands, Elsevier Science, p. 257–301.

Miller, J.D., Jr., and Weiblen, P.W., 1990, Anorthositic rocks of the Duluth Complex: Examples of rocks formed from plagioclase crystal mush: Journal of Petrology, v. 31, p. 295–339.

Miller, J.D., Jr., Green, J.C., Severson, M.J., Chandler, V.W., Hauck, S.A., Peterson, D.M., and Wahl, T.E., 2002, Geology on mineral potential of the Duluth Complex and related rocks of northeastern Minnesota: Minnesota Geological Survey Report of Investigation, v. 58, p. 1–207.

Naldrett, A.J., 1999, World-class Ni-Cu-PGE deposits: Key factors in their genesis: Mineralium Deposita, v. 34, p. 227–240.

——2010, Secular variations of magmatic sulfide deposits and their source magmas: Economic Geology, v. 105, p. 669–688.

O'Neill, H.S., 2021, The thermodynamic controls on sulfide saturation in silicate melts with application to ocean floor basalts, *in* Moretti, R., and Neuville, D.R., eds., Magma redox geochemistry: New Jersey, Wiley-American Geophysical Union, p. 177–213.

Pasteris, J.D., 1985, Relationships between temperature and oxygen fugacity among Fe-Ti oxides in two regions of the Duluth Complex: The Canadian Mineralogist, v. 23, p. 111–127.

Phinney, W.C., 1972, Duluth Complex, history and nomenclature, *in* Sims, P.K., and Morey, G.B., Geology of Minnesota: A centennial volume: Minnesota, USA, Minnesota Geological Survey, p. 333–334.

Putirka, K.D., 2005, Igneous thermometers and barometers based on plagioclase + liquid equilibria: Tests of some existing models and new calibrations: American Mineralogist, v. 90, p. 336–346.

Queffurus, M., and Barnes, S.-J., 2014, Selenium and sulfur concentrations in country rocks from the Duluth Complex, Minnosota, USA: Implications for formation of the Cu-Ni-PGE sulfides: Economic Geology, v. 109, p. 785–794.

Rao, B.V., and Ripley, E.M., 1983, Petrochemical studies of the Dunka Road Cu-Ni deposit, Duluth Complex, Minnesota: Economic Geology, v. 78, p. 1222–1238.

Rezeau, H., and Jagoutz, O., 2020, The importance of $H_2O$ in arc magmas for the formation of porphyry Cu deposits: Ore Geology Reviews, v. 126, p. 1–14.

Ripley, E.M., 1981, Sulfur isotopic studies of the Dunka Road Cu-Ni deposit, Duluth Complex, Minnesota: Economic Geology, v. 76, p. 610–620.

Ripley, E.M., and Alawi, J.A., 1986, Sulfide mineralogy and chemical evolution of the Babbitt Cu-Ni deposit, Duluth Complex, Minnesota: The Canadian Mineralogist, v. 24, p. 347–368.

Ripley, E.M., and Li, C., 2003, Sulfur isotope exchange and metal enrichment in the formation of magmatic Ni-Cu-(PGE) deposits: Economic Geology, v. 98, p. 635–641.

——2013, Sulphide saturation in mafic magmas: Is external sulphur required for magmatic Ni-Cu-(PGE) ore genesis?: Economic Geology, v. 108, p. 45–58.

Ripley, E.M., Butler, B.K., Taib, N.I., and Lee, I., 1993, Hydrothermal alteration in the Babbitt Cu-Ni deposit, Duluth Complex: Mineralogy and hydrogen isotope systematics: Economic Geology, v. 88, p. 679–696.

Ripley, E.M., Park, Y.-R., Li, C., and Naldrett, A.J., 1999a, Sulphur and oxygen isotopic evidence of country rock contamination in the Voisey's Bay Ni-Cu-Co deposit, Labrador, Canada: Lithos, v. 47, p. 53–68.

Ripley, E.M., Lambert, D.D., and Frick, L.R., 1999b, Re-Os, Sm-Nd, and Pb isotopic constraints on mantle and crustal contributions to magmatic sulfide mineralization in the Duluth Complex: Geochimica et Cosmochimica Acta, v. 62, p. 3349–3365.

Ripley, E.M., Park, Y.-R., Lambert, D.D., and Frick, L.R., 2001, Re-Os isotopic composition and PGE contents of Proterozoic carbonaceous argillites, Virginia Formation, northeastern Minnesota: Organic Chemistry, v. 32, p. 857–866.

Ripley, E.M., Taib, N.I., Li, C., and Moore, C.H., 2007, Chemical and mineralogical heterogeneity in the basal zone of the Partridge River intrusion: Implications for the origin of Cu-Ni sulfide mineralization in the Duluth Complex, midcontinent rift system: Contributions to Mineralogy and Petrology, v. 154, p. 35–54.

Saini-Eidukat, B., Weiblen, P.W., Bitsianes, G., and Glascock, D., 1990, Contrasts between platinum group element contents and biotite compositions of the Duluth Complex Troctolitic and Anorthositic Series rocks: Mineralogy and Petrology, v. 42, p. 121–140.

Samalens, N., Barnes, S.-J., and Sawyer, E.W., 2017, The role of black shales as a source of sulphur and semimetals in magmatic nickel-copper deposits: Example from the Partridge River intrusion, Duluth Complex, Minnesota, USA: Ore Geology Reviews, v. 81, p. 173–187.

Sawyer, E.W., 2014, The inception and growth of leucosomes: Microstructure at the start of melt segregation in migmatites: Journal of Metamorphic Petrology, v. 32, p. 695–712.

Seat, Z., Beresford, S.W., Grguric, B.A., Gee, M.A.M., and Grassineau, N.V., 2009, Reevaluation of the role of external sulfur addition in the genesis of Ni-Cu-PGE deposits: Evidence from the Nebo-Babel Ni-Cu-PGE deposit, West Musgrave, Western Australia: Economic Geology, v. 104, p. 521–538.

Severson, M.J., 1991, Geology, mineralization, and geostatistics of the Minnamax Babbitt Cu-Ni deposit (Local Boy area), Minnesota: Part I: Geology: University of Minnesota, Technical Report NRRI-91/13a, p. 1–99.

Severson, M.J., and Barnes, J.R., 1991, Geology, mineralization, and geostatistics of the Minnamax/Babbitt Cu-Ni deposit (Local Boy area), Minnesota: Part II: Mineralization and geostatistics: University of Minnesota, Technical Report, NRRI-91/13b, p. 1–215.

Severson, M.J., Patelke, R.L., Hauck, S.A., and Zanko, L.M., 1996, The Babbitt copper-nickel deposit part C: Igneous geology, footwall lithologies, and cross-sections: University of Minnesota, Technical Report NRRI-94, p. 1–68.

Shima, H., and Naldrett, A.J., 1975, Solubility of sulfur in an ultramafic melt and the relevance of the system Fe-S-O: Economic Geology, v. 70, p. 960–967.

Smythe, D.J., Wood, B.J., and Kiseeva, E.S., 2017, The S content of silicate melts at sulfide saturation: New experiments and a model incorporating the effects of sulfide composition: American Mineralogist, v. 102, p. 795–803.

Swanson-Hysell, N.L., Hoaglund, S.A., Crowley, J.L., Schmitz, M.D., Zhang, Y., and Miller, Jr., J.D., 2021, Rapid emplacement of massive Duluth Complex intrusions within the North American Midcontinent rift: Geology, v. 49, p. 185–189.

Thériault, R.D., and Barnes, S.-J., 1998, Compositional variations in Cu-Ni-PGE sulphides of the Dunka Road deposit, Duluth Complex, Minnesota; the importance of combined assimilation and magmatic processes: The Canadian Mineralogist, v. 36, p. 869–886.

Tyson, M.R., and Chang, L.L.Y., 1984, The petrology and sulphide mineralization of the Partridge River troctolite, Duluth Complex, Minnesota: The Canadian Mineralogist, v. 22, p. 23–38.

Virtanen, V.J., Heinonen, J.S., Molnár, F., Schmidt, M.W., Marxer, F., Skyttä, P., Kueter, N., and Moslova, K., 2021, Fluids as primary carriers of sulphur and copper in magmatic assimilation: Nature Communications, v. 12, 12 p., doi: 10.1038/s41467-021-26969-3.

Weiblen, P.W., and Morey, G.B., 1980, A summary of the stratigraphy, petrology, and structure of the Duluth Complex, Minnesota: American Journal of Science, v. 280-A, p. 88–133.

Wieser, P.E., Jenner, F., Edmonds, M., Maclennan, J., and Kunz, B.E., 2020, Chalcophile elements track the fate of sulfur at Kīlauea volcano, Hawai'i: Geochimica et Cosmochimica Acta, v. 282, p. 245–275.

Yao, Z.-S., and Mungall, J.E., 2021, Linking the Siberian flood basalts and giant Ni-Cu-PGE sulfide deposits at Norilsk: Journal of Geophysical Research, v. 126, p. 1–22.

**Ville J. Virtanen** is a doctoral student at the Department of Geosciences and Geography at the University of Helsinki. His research focuses on various aspects of magmatic assimilation, including the reactions that mobilize and transport sulfur and metals in the wall rock and the effect that the introduced foreign material has on the magma. To improve the understanding of these processes, he seeks to combine observations from the natural systems with experimental petrology and computational thermodynamic modeling.